REPORT DOCUMENTATION PAGE

Form Approved
OMB No. 0704-0188

1. AGENCY USE ONLY *(Leave blank)*	2. REPORT DATE	3. REPORT TYPE AND DATES COVERED
	9.Mar.04	THESIS

4. TITLE AND SUBTITLE
MODEL AND DESIGN CONSTANT MODULATION CURRENT BIAS CIRCUIT FOR MEASURING THE SMALL SIGNAL RESPONSE OF SEMICONDUCTOR LASERS

5. FUNDING NUMBERS

6. AUTHOR(S)
2D LT VAP JASON C

7. PERFORMING ORGANIZATION NAME(S) AND ADDRESS(ES)
UNIVERSITY OF WYOMING

8. PERFORMING ORGANIZATION REPORT NUMBER
CI04-136

9. SPONSORING/MONITORING AGENCY NAME(S) AND ADDRESS(ES)
THE DEPARTMENT OF THE AIR FORCE
AFIT/CIA, BLDG 125
2950 P STREET
WPAFB OH 45433

10. SPONSORING/MONITORING AGENCY REPORT NUMBER

11. SUPPLEMENTARY NOTES

12a. DISTRIBUTION AVAILABILITY STATEMENT
Unlimited distribution
In Accordance With AFI 35-205/AFIT Sup 1

12b. DISTRIBUTION CODE

13. ABSTRACT *(Maximum 200 words)*

14. SUBJECT TERMS

15. NUMBER OF PAGES
98

16. PRICE CODE

17. SECURITY CLASSIFICATION OF REPORT	18. SECURITY CLASSIFICATION OF THIS PAGE	19. SECURITY CLASSIFICATION OF ABSTRACT	20. LIMITATION OF ABSTRACT

MODEL AND DESIGN OF A CONSTANT MODULATION CURRENT BIAS CIRCUIT FOR MEASURING THE SMALL SIGNAL RESPONSE OF SEMICONDUCTOR LASERS

by
Jason C. Vap

A thesis submitted to the Department of Electrical and Computer Engineering
and The Graduate School of the University of Wyoming
in partial fulfillment of the requirements
for the degree of

MASTER OF SCIENCE
in
ELECTRICAL ENGINEERING

Laramie, Wyoming
May, 2004

Vap, Jason C., Model and Design of a Constant Modulation Bias Circuit for Measuring the Small-Signal Response of Semiconductor Lasers, M.S., Department of Electrical and Computer Engineering, May, 2004.

The goal of this thesis was to design a constant modulation current bias circuit for measuring the single-pole, small-signal optical response of a semiconductor laser between 1MHz and 1GHz. The results of this design will be used to conduct carrier lifetime measurements with the impedance independent optical response technique—essential for determining the carrier density in the active region of the semiconductor laser, and extracting the A, B, and C coefficients of the spontaneous recombination rate equation.

We first approached the design through modeling the impedance of the components based on the parasitic information given in the manufacturer's data sheets, and using best guesses for the parasitic information not given. This method failed due to an underestimation of the parasitic capacitance coming from the substrate material of the surface mount chip resistors; this caused an increasing modulation current to be delivered to the laser above 200MHz. Thus, we moved to a second design approach.

In this design approach, we directly measured the impedance of each component through performing forward transmission (S21) measurements using a network analyzer. The results of these measurements placed an upper boundary on the size of resistor (430Ω) we could use up to 1GHz. Therefore, we used the S21 measurements to successfully design two constant modulation current bias circuits: a *low frequency bias circuit* used at low laser bias levels where the impedance of the laser is large and the single-pole, small-signal response resides at lower frequencies (~1MHz to 100MHz); and a *high frequency bias circuit* used at higher laser bias levels where the impedance of the laser is low and the single-pole, small-signal response resides at higher frequencies (~100MHz to 1GHz).

Vap, Jason C., Model and Design of a Constant Modulation Bias Circuit for Measuring the Small-Signal Response of Semiconductor Lasers, M.S., Department of Electrical and Computer Engineering, May, 2004.

The goal of this thesis was to design a constant modulation current bias circuit for measuring the single-pole, small-signal optical response of a semiconductor laser between 1MHz and 1GHz. The results of this design will be used to conduct carrier lifetime measurements with the impedance independent optical response technique—essential for determining the carrier density in the active region of the semiconductor laser, and extracting the A, B, and C coefficients of the spontaneous recombination rate equation.

We first approached the design through modeling the impedance of the components based on the parasitic information given in the manufacturer's data sheets, and using best guesses for the parasitic information not given. This method failed due to an underestimation of the parasitic capacitance coming from the substrate material of the surface mount chip resistors; this caused an increasing modulation current to be delivered to the laser above 200MHz. Thus, we moved to a second design approach.

In this design approach, we directly measured the impedance of each component through performing forward transmission (S21) measurements using a network analyzer. The results of these measurements placed an upper boundary on the size of resistor (430Ω) we could use up to 1GHz. Therefore, we used the S21 measurements to successfully design two constant modulation current bias circuits: a *low frequency bias circuit* used at low laser bias levels where the impedance of the laser is large and the single-pole, small-signal response resides at lower frequencies (~1MHz to 100MHz); and a *high frequency bias circuit* used at higher laser bias levels where the impedance of the laser is low and the single-pole, small-signal response resides at higher frequencies (~100MHz to 1GHz).

Acknowledgements

I would like to thank Dr. Jon Pikal and Dr. Eva Ferre-Pikal for their assistance and their patience during the past 17 months. Research work is an extraordinary challenge, and my hat goes off to both of you for your level of commitment and drive. Next, I would like to thank Amit Dikshit and Vishnu Vangapally for their help in the lab and for educating me on the traditions and history of India. You both have extraordinary personalities, and it was a pleasure to get to know you both. I would also like to thank Scott Jacobs for his assistance in the lab, and helping me laugh more.

Finally, I would like to thank Clarence and Dennis. You guys kept me company in the mornings when no one else was around. It was also a pleasure to get to know you gentlemen, and I wish you the best of luck and wellness in the future.

Note: The views expressed in this thesis are those of the author and do not reflect the official policy or position of the United States Air Force, Department of Defense, or the U.S. Government.

Table of Contents

List of Figures

Chapter 1

Chapter 2

Chapter 3

Chapter 4

Chapter1

Introduction

The concept of an electrically driven semiconductor laser was first introduced by Popov and Bosov in 1961, who suggested that stimulated emission of radiation could occur in semiconductor lasers through the recombination of carriers injected across a p-n junction [1,2]. Shortly following this, the first semiconductor lasers were produced and lasing was achieved (1962). Despite this achievement, the progress in semiconductor lasers remained slow for the next few years; this was because the mature semiconductor process of this time was silicon—an indirect bandgap material. Semiconductor lasers require direct bandgap material which is found in compound semiconductors, which were not well understood at the time [1].

Without a mature compound semiconductor process, the lasers produced at this time suffered from high threshold currents and limited the laser operation to short pulses at cryogenic temperatures [1]. It was not until the advent of heterostructures[1] in 1969 that the first semiconductor lasers were able to operate continuous wave (cw) at room temperature [1]. Following this, the next big breakthrough in semiconductor lasers came from Dingle and Henry in 1976, who introduced the idea of exploiting the quantum effects of heterostructure semiconductor lasers to yield wavelength tunability and achieve lower lasing thresholds [4].

The concept of wavelength tunablity comes from using the disparities in the bandstructure of semiconductor materials to not only confine the carriers to a particular region in the laser, but to also restrict one or more dimensions of the confinement to less than the de Broglie wavelength of an electron. This yields a quantization in the energy of the

[1] Heterostructures refer to the bandgap disparities between semiconductor materials grown juxtapose [3].

carriers found in this region, effectively tuning the carriers to a specific energy or equivalently a specific wavelength.

As for exploiting the quantum effects in lasers to achieve lower threshold currents, this is accomplished through reducing the density of states of our carriers—effectively where we can park our charged carriers in energy. Figure 1.1 is an illustration of the density of states for charged carriers with varying degrees of freedom—from 3-D down to 0-D. From this figure, we see that the restrictions in the density of states are concomitant with the restrictions placed on the available degrees of freedom to our carriers.

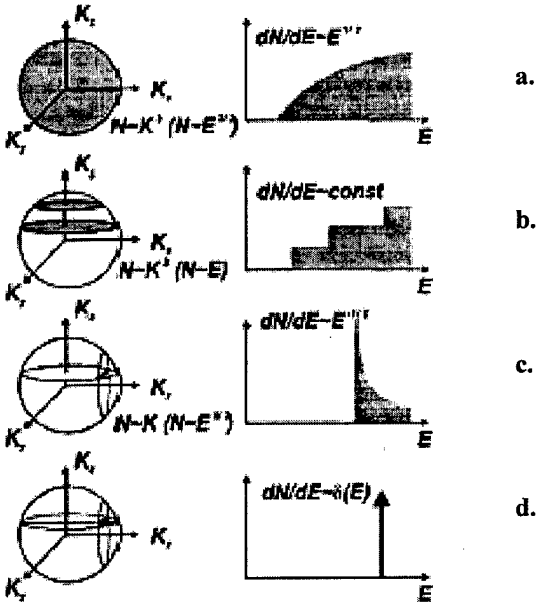

Figure 1. Density of states with following degrees of freedom **a.** 3-d (bulk material) **b.** 2-d (quantum well) **c.** 1-d (quantum wire) **d.** 0-d (quantum dot) [4].

Examining figure 1.1 further, we see that the area below the curves in figures 1.1a through 1.1d represent where the charged carriers can reside in energy due to the restrictions placed on their translational degrees of freedom. Starting with the bulk case (figure 1.1a), we see that the density of states is a continuous function of energy. However, when we move to the quantum well case (figure 1.1b), we see the density of states becomes restricted—it is no longer a continuous function of energy rather it is step-like. Moving onto the quantum wire

case (figure 1.1c), we see a further restriction in the density of states in energy. Finally, when we move to the quantum dot case (figure 1.1d), we observe a delta-like density of states.

The result of the restrictions in the density of states is an increasingly narrow energy range near the bottom of the conduction band and/or top of the valence band [4]. This is precisely how Dingle and Henry proposed reducing the threshold currents of lasers. For if the energy parking spots of our carriers are forced to reside at the conduction and valence band edges, the maximum material gain is enhanced, and the temperature performance of the device is also enhanced [4]. Both of these enhancements ultimately yield reductions in the threshold current of semiconductor lasers. Figure 1.2 illustrates the trend in threshold currents of double heterostructure, quantum well, and quantum dot lasers since the advent of each.

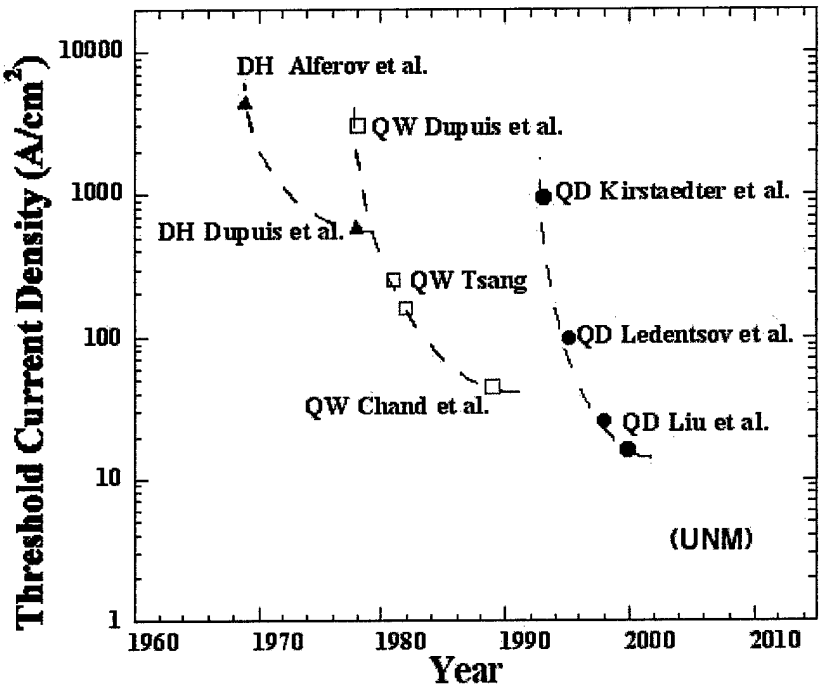

Figure 2. Progress of threshold currents of double heterostructure, quantum well, and quantum dot lasers [5].

So far, we have tracked the progress of semiconductor lasers through history. However, we have not yet discussed why we are so interested in them. Semiconductor lasers have become highly efficient, compact in size, possess the longest lifetime of all existing lasers, and they can be directly modulated—each of these characteristics makes them appealing to optical-fiber communication [1]. The popularity of semiconductor lasers in long haul optical-fiber communication has motivated the development of semiconductor lasers operating at 1.3μm, the zero dispersion wavelength in optical fibers, and 1.55μm, the minimum loss wavelength in optical fibers [3,6]. A lot of the present focus on semiconductor laser research revolves around the temperature dependence of the threshold current in these long wavelength lasers [6].

It is true that semiconductor lasers are capable of operating cw at room temperature; however, when these devices are operated for long periods of time at current densities above threshold they suffer from self-heating. This, in-turn, can shift the threshold current to higher and higher values, and it can also shift the operating wavelength of the laser—both detrimental effects to a fiber optic communication system. To avoid these effects, semiconductor lasers used in long haul optical fiber communication are actively cooled, further increasing the costs of these systems [6,7].

For the time being, we are actively cooling these semiconductor lasers in order to "treat the symptoms" of the laser's threshold current temperature dependence. Meanwhile, a great deal of effort is being put forth in order to determine the root cause of this temperature dependence. In order for us to get a handle on the temperature dependence of the threshold current, we must identify the *recombination mechanisms* making up the threshold current as well as the *gain* and *loss* properties responsible for establishing the carrier density in which we achieve lasing [6].

Gain can be measured without direct knowledge of the carrier density; however, the material gain parameters dg/dn (differential gain), and n_{tr} (the transparency carrier density) require direct knowledge of the carrier density in the active region of the laser. The recombination mechanisms (defect, radiative, and Auger) also follow a carrier density dependency, and performing carrier lifetime measurements is the most direct method for both determining the carrier density in the active region, and examining the recombination processes occurring inside the laser [6,8].

There are several different methods used to extract carrier lifetimes [6,9,10,11]; however, this thesis focuses on the impedance independent optical response technique [6,11]. We specifically focus on the design of the bias tee circuit used in this technique, which is responsible for supplying a constant small-signal modulation current to the semiconductor laser. As for the contents of this thesis, chapter 2 presents some background information on semiconductor lasers and the high frequency models of the components used in the bias tee circuit design, in order to adequately prepare the reader for the details of the design processes. The two chapters following this (chapters 3 and 4) concentrate on the two different design approaches taken to obtain a constant small-signal modulation current delivery to the semiconductor laser. Chapter 3 examines a data sheet design of the bias tee circuit and points out why we pursued another design route—the first bias tee circuit was delivering a constant modulation current from 200MHz to 1GHz. Chapter 4 examines the second design approach and how we solved the increasing modulation current issue from the first design. The final chapter (chapter 5) presents some concluding remarks on the two designs.

References—Chapter 1

[1] W.W. Chow, S.W. Koch, "Semiconductor-Laser Fundamentals," Springer-Verlag Berlin Heidelberg New York, 1999.

[2] N.N. Ledentsov, "Long-Wavelength Quantum-Dot Lasers on GaAs Substrates: From Media to Device Concepts," IEEE Journal of Selected Topics in Quantum Electronics, Vol. 8, No. 5, Sept/Oct 2002.

[3] P. Bhattacharya, "Semiconductor Optoelectronic Devices," Prentice Hall, 1997.

[4] N.N. Ledentsov, et al., "Quantum Dot Heterostructure Lasers," IEEE Journal of Selected Topics in Quantum Electronics, Vol. 6, No. 3, May/June 2000.

[5] http://www.zialaser.com/technology.html

[6] J.M. Pikal, "Temperature Dependence of Carrier Lifetime, Recombination, and Gain in 1.3μm InAsP/InGaAsP Multiple Quantum Well Lasers," Dissertation, Aug. 1999.

[7] http://www.samhassan.com/IntroductionstoFiberOpticalCommunications.htm.

[8] R. Olshansky, et al., "Measurement of Radiative and Nonradiative Recombination Rates in InGaAsP and AlGaAs Light Sources," IEEE JQE, Vol. QE-20, No. 8, Aug 1984.

[9] R.W. Dixon and W.B. Joyce, "Generalized Expressions for the Turn-On-Delay in Semiconductor Lasers," J. Appl. Phys., Bol. 50, no.7, pp. 4591-4595, 1979.

[10] G.E. Shtengel, et. al., "Impedance-Corrected Carrier Lifetime Measurements in Semiconductor Lasers," Appl. Phys. Letters, Vol. 67, No. 11, 1506-1508, 1995.

[11] J.M. Pikal and C.S. Menoni, "Impedance Independent Optical Carrier Lifetime Measurements in Semiconductor Lasers," Review of Scientific Instruments, Vol. 69, No. 12, 4247-4248.

Chapter 2

Background

2.1 Introduction

The basis of this chapter is to expose the reader to the terms and concepts needed to understand the work completed in this thesis and is broken into 5 sections. The first section covers *semiconductor laser fundamentals*: it explores the essential elements of a semiconductor laser, the edge-emitting laser and its structure, types of photon-carrier processes, light output vs. current injection curves, and finally the laser rate equations. The second section covers *carrier lifetimes*: it will specifically delve into the spontaneous recombination rate equation, and explain why we are so interested in taking below threshold carrier lifetime measurements. The third section covers the *impedance independent optical response technique*: it will examine the experimental setup of this technique, explain why we need to deliver a constant small-signal modulation current to the laser, and finally examine the operating characteristics of the bias tee circuit. Specifically, we will look at how it delivers a constant small-signal modulation current to the semiconductor laser. The fourth section is *high-frequency models and the semiconductor laser equivalent circuit*: it examines the high frequency models of each component used in the bias tee circuit, and it also describes the equivalent circuit for the semiconductor laser. The fifth section is the *design approaches*: it introduces the two separate design approaches for the bias tee circuit used in this research before they are entirely revealed in chapters 3 and 4.

2.2 Semiconductor Laser Fundamentals

The three essential elements needed for any type of laser (gas, solid state, or semiconductor) are: a *pump*, a *gain medium*, and *positive feedback* [1]. We will limit our discussion here to the sources responsible for each of these mechanisms in edge-emitting

semiconductor lasers—the type of lasers used in this research. First, the *pump* is provided through forward biasing the semiconductor laser diode with a battery or a current source; this injects both electrons and holes into the second essential element—the *gain medium.* The *gain medium* is the active region of a laser; this is where photons and carriers (electrons and holes) are confined and allowed to interact with one another—the exact processes will be addressed in the photon-carrier processes portion of this section. The final essential element of a laser is *positive feedback.* This element is provided by the cleaved facets at both ends of the edge-emitting semiconductor laser—the uncoated facet reflectivities are approximately 30%, due to the abrupt change in the refractive index seen by photons when they reach the semiconductor-air interface present at each facet [2]. The role of the positive feedback element is to setup self-sustaining oscillations (standing waves) within the laser cavity; this is accomplished through reflecting a portion of the light traveling through the laser cavity back into the laser's cavity [1]. Through doing this, the laser will interact with the carriers injected by the pump and provide a continuous output power for a given bias or current injection level. The following figures illustrate the three essential elements of an edge-emitting semiconductor laser.

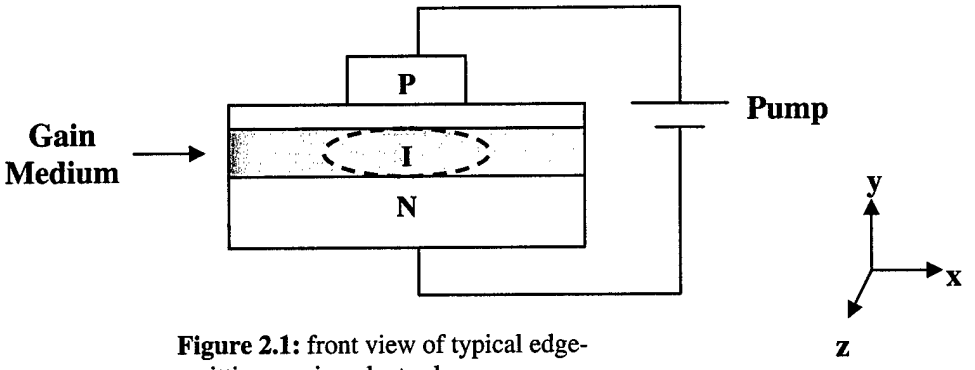

Figure 2.1: front view of typical edge-emitting semiconductor laser.

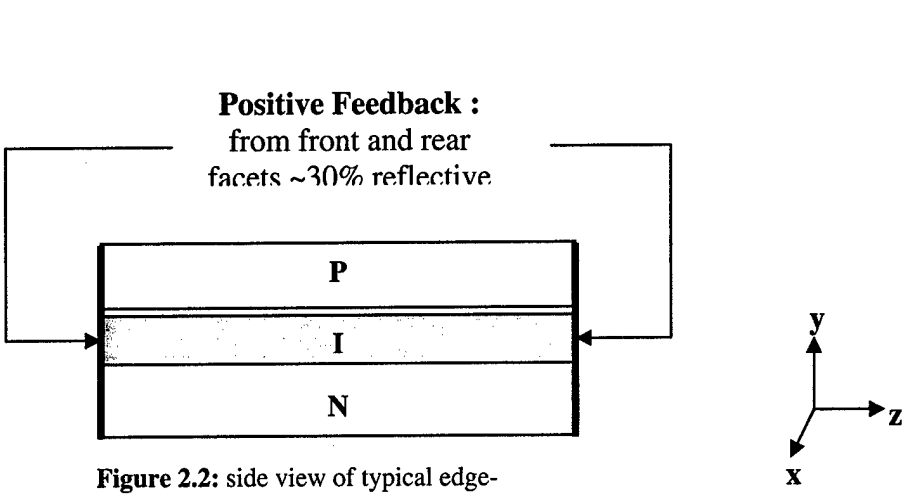

Figure 2.2: side view of typical edge-emitting semiconductor laser.

2.2.1 Edge-Emitting Lasers

The types of lasers illustrated in figures 2.1 and 2.2 are edge-emitting ridge waveguide lasers. The edge-emitting lasers used in this research were quantum dot lasers manufactured at the University of Texas at Austin at the Microelectronics Research Center by Dr. O. B. Shchekin and D. G. Deppe [3]. The stripe widths ranged from 1μm to 58μm, and the cleaved lengths ranged from 1mm to 2mm.

The region of the edge-emitting laser in which we observe the light output beam can be seen in figure 2.1—it is the dotted oval region on the facet. Light is emitted from this region because the physical features of the edge-emitting laser are designed such that photons prefer to travel in a longitudinal direction (z-direction) along the resonant cavity of the active region. This preference is induced by the lack of gain and no reflection or feedback in the x-direction and the lower index of refraction in both the x and y-directions.

2.2.2 Edge-Emitting Laser Structure

Now, we will examine the three physical features of the edge-emitting laser diode seen in figure 2.3: the *P*, *I* and *N* regions.

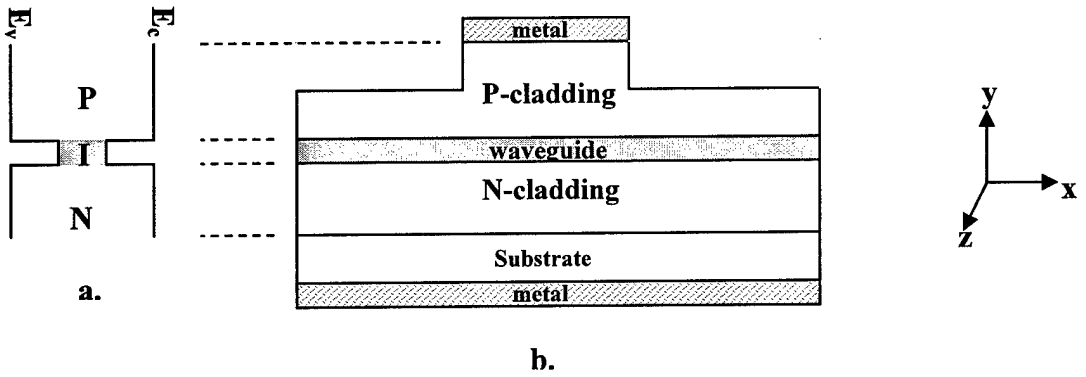

Figure2. 3: a.) Band diagram of cladding and waveguide regions
b.) Simplified layer structure of an edge-emitting laser.

The *P* region is semiconductor material that is highly doped with acceptor atoms; the *I* region is intrinsic semiconductor material (no doping); and the *N* region is semiconductor material highly doped with donor atoms. Through forward biasing this structure, holes from the P-region and electrons from the N-region are injected into the intrinsic region of the laser. Once the carriers are injected into the intrinsic region, they become confined due to the band structure (see figure 2.3a). This confinement forces the injected electrons and holes to reside in the same region of space (a potential well), ultimately leading to light producing recombination events.

Further examination of figure 2.3b presents some of the details as to how photons, once they are produced, remain confined (relatively) to the active region. The cladding regions surrounding the waveguide region possess a lower index of refraction than the waveguide region; thus, photons are guided down the active region of the laser due to the index of refraction differences imposed by the P and N regions surrounding the active region of the laser. The index of refraction (η) follows an inverse bandgap (the difference in the conduction band E_c and valence band E_v energies) dependence obeying Moss' Rule; an empirical relationship obeyed by semiconductors with η^4 falling between 30 to 440 [4].

$$\eta = \left(\frac{77}{E_g} \right)^{\frac{1}{4}}$$

Eqn 1. Moss' Rule for index of refraction bandgap dependence [4]

Thus, we see it is rather fortuitous that the bandgap disparities responsible for confining our carriers are also responsible for confining photons to the intrinsic region—later we will see that the volume occupied by the photons divided by the volume occupied by the carriers is known as the optical confinement factor and is important in determining gain. Now, we are ready to discuss the types of photon-carrier interactions occurring inside the laser.

2.2.3 Types of Photon-Carrier Processes:

Semiconductor lasers exhibit three photon-carrier processes: *spontaneous emission*, *stimulated emission*, and *stimulated absorption*, often referred to as just absoption; each of these processes can be observed in figure 2.4 [5]. First, *spontaneous emission* occurs when an electron in the conduction band (CB) falls to the valence band (VB), without the assistance of an incident photon, and recombines with a hole; the excess energy of this process is given off as a photon of light, which has a random direction and phase. *Stimulated emission* occurs when an incident photon in the active region of a laser perturbs (stimulates) the electromagnetic field of an electron in the CB, causing it to fall to the VB. Again, the excess energy is given off as a photon of light, but there is also something remarkable about this process. The photon produced is identical to the stimulating photon: same frequency, phase, and direction of propagation—what is called coherent light. Stimulated emission also has an inverse process—*stimulated absorption.* This occurs when an incident photon perturbs the electromagnetic field of an electron in the VB; a coupling event occurs in which the energy of the photon is transferred to the electron causing it to rise in energy to the CB—the photon is annihilated in this process [5]. All three of these processes occur in the laser cavity under forward biased conditions; however, it is the level of population inversion

(controlled by the level of laser biasing) that establishes which process is dominant. Population inversion is the condition in which there are more carriers residing in the excited state than in the ground state.

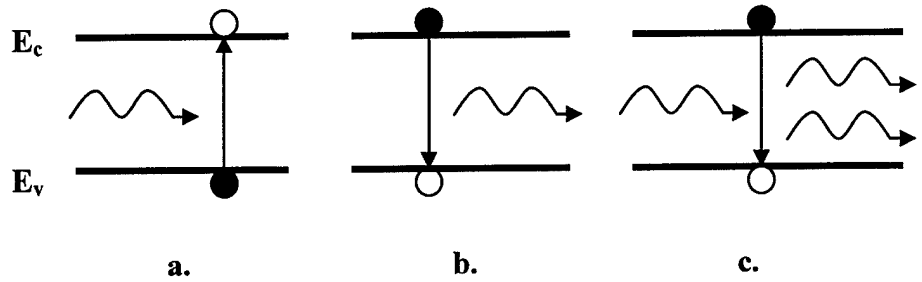

Figure 2.4: a.) stimulated absorption, **b.)** spontaneous emission **c.)** stimulated emission

2.2.4 Light vs. Current Characteristics

Figure 2.5 is an illustration of a light power versus injection current curve. From this figure, we observe two regions of laser operation: below threshold, and above threshold. The transition point between these two regions occurs at the threshold current I_{th}—the amount of current needed for the laser to begin lasing, or begin producing predominantly coherent light. Now, the reason for two different regions of laser operation is due to the processes or process dominant in that region. In the below threshold region, the dominant processes are stimulated absorption and spontaneous emission events. At the transition point (I_{th}) and beyond, we move into the above threshold region where the carrier density in the active region becomes *pinned* at n_{th} and stimulated emission becomes the dominant process. Carriers injected into the active region of the laser in excess of n_{th} are immediately removed by the stimulated emission process, restoring the carrier density to n_{th} [5]. Thus, we observe a steep, linear dependence of the light output with injected current above threshold. In order to understand this dependence, we must examine the laser rate equations.

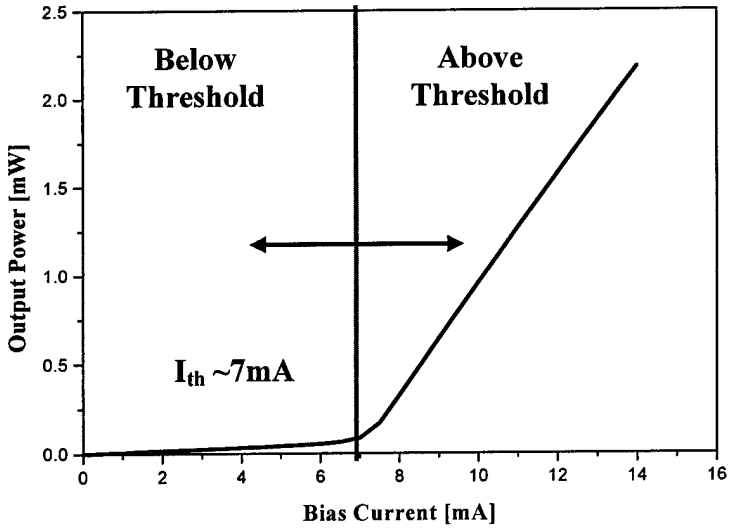

Figure 2.5: Light versus Current curve

2.2.5 Laser Rate Equations

The laser rate equations are a coupled set of differential equations, each responsible for keeping track of the dynamic processes occurring inside the laser; they are the carrier density rate equation, and the photon density rate equation.

$$\frac{dn}{dt} = \frac{\eta_i I}{qV} - \frac{n}{\tau(n)} - v_g a(n - n_{tr})s$$

Eqn 2. Carrier density rate equation
Units: carriers/(cm^3sec)

The carrier density rate equation keeps track of the carriers coming into and exiting the active region of the laser. The first term on the right is the carrier injection term (electrons n or holes p): I is the total current injected into the laser, η_i is the injection efficiency (the fraction of the injected carriers making it to the active region), q is the charge of an electron, and V is the active region volume. The second term of the carrier density rate equation is the spontaneous recombination rate term (eqn3): n is the carrier density, and τ is the carrier lifetime.

$$R = \frac{n}{\tau(n)} = An + Bn^2 + Cn^3$$

Eqn 3. Spontaneous Recombination Rate

The spontaneous recombination rate term represents an effective decay of the carriers (average time the carriers live in the laser) through three different recombination processes: *defect recombination*[1] (represented by the A coefficient and sometimes referred to as Shockley-Hall-Reed recombination), *radiative recombination*[2] (B), and *Auger recombination*[3](C); we will examine each of these processes carrier density dependency in the carrier lifetime section. The last term of the carrier density rate equation is the stimulated emission term: where υ_g is the group velocity, a is the differential gain (dg/dn), n is the carrier density and n_{tr} is the transparency carrier density (the carrier density at which the probability of a photon absorption event and a stimulated emission event are equally likely), finally s is the photon density [5]. One final note on the carrier density rate equation is the sign of each term: current injection increases the carrier density in the active region (positive sign out front); the spontaneous recombination decreases the carrier density in the active region (negative sign out front); and finally stimulated emission decreases the carrier density in the active region (negative sign out front).

$$\frac{ds}{dt} = \Gamma v_g a(n - n_{tr})s + \beta\frac{n}{\tau(n)} - \frac{s}{\tau_p}$$

Eqn 4. Photon density rate equation
Units: photons/(cm^{3}sec)

The photon density rate equation keeps track of the photons created and the photons exiting the active region of the laser. The first term of the photon density rate equation is the stimulated emission term: Γ is the optical confinement factor (effectively the volume occupied by the light V_p divided by the volume occupied by the carriers V); v_g is the group velocity of the photons, a is the differential gain, n is the carrier density, n_{tr} is the transparency carrier density, and s is the photon density. The second term in this expression

[1] Defect recombination—nonradiative carrier recombination mechanism due to defects in the active region [5].
[2] Radiative recombination—light emitting process due to spontaneous emission [5].
[3] Auger recombination—nonradiative carrier recombination mechanism involving three carriers. In this process, an electron recombines with a hole; the excess energy is not given off as a photon of light, but rather it is transferred to another electron or hole kicking that carrier higher in its respective band [5].

represents the amount of spontaneous emission coupling into the lasing mode: β is the spontaneous emission factor, n is the carrier density, and τ is the carrier lifetime. The final term of the photon density rate equation is the photon decay term: s is the photon density, and τ_p is the photon lifetime. The photon decay term accounts for optical losses both inside the cavity and at the facets [5]. One final note on the photon density rate equation is the sign of each term: stimulated emission increases the photon density in the active region (positive sign out front); spontaneous emission into the lasing mode increases the photon density in the active region (positive sign out front); and photon losses both in the cavity and at the facets decrease the photon density in the active region (negative sign out front).

Presently, we need to examine the laser rate equations in greater detail to answer two questions: **1.)** Why does the light output of the laser behave linearly with the injected current above threshold; and most importantly, **2.)** Why do we want to take below threshold carrier lifetime measurements. To answer the first question, we must go back to the carrier density rate equation (eqn2) and solve for the spontaneous recombination rate term very close to threshold. To do this we make two assumptions: the carrier density is n_{th}, and the stimulated emission term is still negligible in comparison to the spontaneous emission term. Through making these two assumptions and making the observation in steady state (time derivatives go to zero), the carrier density rate can be solved for the spontaneous recombination rate.

$$\frac{n_{th}}{\tau(n_{th})} = \frac{\eta_i I_{th}}{qV}$$

Eqn. 5 Spontaneous recombination rate near threshold

Now, we can make this substitution into the carrier density rate equation, and refer to it as the above threshold carrier density rate equation [5].

$$\frac{dn}{dt} = \frac{\eta_i (I - I_{th})}{qV} - v_g a(n_{th} - n_{tr})s$$

Eqn. 6 Carrier density rate equation above threshold

Before we jump into the above threshold photon density rate equation, we need to make two definitions: the photon lifetime τ_p, and the modal threshold gain Γg_{th}. First, the photon lifetime is composed of two lifetimes: the internal loss lifetime due to photons being lost inside the laser cavity to absorption or scattering events, and the mirror loss lifetime due to photons leaving the laser cavity via the facets [5]. With this noted, the following photon lifetime definition can be made.

$$\frac{1}{\tau_p} = \frac{1}{\tau_i} + \frac{1}{\tau_m} = v_g(\alpha_i + \alpha_m)$$ **Eqn. 7 Photon lifetime definition**

After defining the photon lifetime in terms of the internal loss lifetime (τ_i) and the mirror loss lifetime (τ_m), we set it equal to the internal losses (α_i) and mirror losses (α_m) multiplied by the group velocity (υ_g) [5]. The units on the internal and mirror loss terms are cm^{-1}, where the mirror losses are considered a distributed parameter over the laser cavity length in order to obtain units consistent with the internal loss term. With the photon lifetime defined, we can move onto defining the modal threshold gain.

At the laser threshold, the modal gain is pinned at a value (Γg_{th}) equal to the internal and mirror losses of the laser [5]. The threshold modal gain is defined in the following way.

$$\Gamma g_{th} = \alpha_i + \alpha_m = \frac{1}{v_g \tau_p}$$ **Eqn. 8 Threshold modal gain definition**

It is the saturation in the gain (ultimately owing its dependence on the carrier density saturation) of the laser at threshold and above that yields the linear dependence in the photon density in the active region of the laser. Since there is a linear dependence of the photon density in the active region of the laser, we will identically observe a linear dependence in the light output of the laser. We are now prepared to examine the photon density rate equation at steady state above threshold—specifically, we want to solve for the photon

density above threshold as this will allow us to obtain the output power of the laser as a function of bias current.

$$s = \frac{\eta_i (I - I_{th})}{q g_{th} v_g V}$$

Eqn. 9 Photon density in the active region above threshold

The structure of this equation is obtained from examining the above threshold carrier density rate equation in steady state (eqn 6): First, solve eqn 5 for the stimulated emission term and then substitute that term into the steady state photon density rate equation (eqn 4 with left-hand-side equal to zero). Once this substitution is made, we proceed by neglecting the spontaneous emission term in the steady state photon density rate equation since the amount of spontaneous emission coupled into the lasing mode is very small. The final step is to solve for the photon density and substitute $v_g \Gamma g_{th}$ for $1/\tau_p$—this is how you get to the final form of eqn 9 [5]. Now that we have the photon density in the active region above threshold, we will proceed to determining the output power of the laser above threshold.

The output power of the laser can be obtained through investigating the amount of optical energy stored in the active region of the laser. This is done through multiplying the photon density by the volume occupied by the photons (V_p) and the energy per photon ($h\upsilon$) [5]. Therefore the stored optical energy in the active region of the laser becomes

$$E_{os} = V_p h v s .$$

Eqn. 10 Optical energy stored in the active region of the laser

After making this assertion, we multiply the stored energy by the energy loss rate from the facets (mirrors) to obtain the optical power output from the mirrors.

$$P_o = v_g \alpha_m s h v V_p$$

Eqn. 11 Intermediate equation for optical power

Now, we substitute the photon density from eqn 8 and the threshold gain g_{th} from eqn 8 into eqn 9 to arrive at the following output power equation [5].

$$P_o = \eta_i \left(\frac{\alpha_m}{\alpha_i + \alpha_m} \right) \frac{hv}{q} (I - I_{th})$$

Eqn. 12 Intermediate equation for optical power

Now, we make one last definition before we obtain the final optical power equation—the differential quantum efficiency.

$$\eta_d = \eta_i \left(\frac{\alpha_m}{\alpha_i + \alpha_m} \right)$$

Eqn. 13 Differential quantum efficiency

From this equation, we can see that the differential quantum efficiency tells us the percentage of the total carriers injected into the laser, which are expected to leave the laser as photons of light above threshold. With this definition made, we can finally develop the *total* optical power coming out of the laser.

$$P_o = \eta_d \frac{hv}{q} (I - I_{th})$$

Eqn. 14 Total optical power output Equation: both facets

If we want the power coming from a single facet of the laser, we need to divide this equation by two—this is precisely the optical power expected to be seen by a photodetector if we could capture and focus all of the light coming from a single facet of the laser. From the functional form of eqn 13, we finally see the output power of the laser behaves linearly with injected current above threshold—again, it is due to pinning of the gain above threshold. Therefore, we will now enter a new section dedicated to answering the second question posed earlier: Why do we want to take below threshold carrier lifetime measurements.

2.3 Carrier Lifetimes

Taking carrier lifetime measurements is the most direct method for determining the carrier density in the active region, and extracting the spontaneous recombination rate coefficients [6]. It is important to know the carrier density in the active region because several laser parameters exhibit a dependence on carrier density: the transparency carrier density n_{tr}, the index of refraction, and material gain dg/dn [6]. It is also important to extract

the coefficients of the spontaneous recombination rate equation, as this enables us to explain the level of contribution each recombination process has on the threshold current density [6]. Additionally, the temperature dependence of these processes can also be investigated. This is done to establish a correlation between the temperature dependence of one of the recombination processes and the temperature dependence of the threshold current of semiconductor lasers [6]. At this point, we need to examine the spontaneous recombination rate equation again (eqn 15); this time discussing each of the recombination processes carrier density dependency.

$$R = \frac{n}{\tau(n)} = An + Bn^2 + Cn^3$$ **Eqn. 15 Spontaneous recombination rate equation**

The three recombination processes (*defect*, *spontaneous*, and *Auger*) mentioned in the laser rate equations section are all accounted for in this equation. *Defect* recombination is accounted for by the A coefficient and is a process involving a single carrier—thus we see n to the first power. *Spontaneous* recombination is accounted for by the B coefficient and is a process involving two carriers—thus we see n to the second power. *Auger* recombination is accounted for by the C coefficient and is a process involving three carriers—thus we see n to the third power [5]. Finally, the reason we can get away with using just n in the spontaneous recombination rate equation is due to the charge neutrality assumption for an undoped or intrinsic active region. For every electron (n) injected into the active region, we must identically inject a hole (p) in order to maintain charge neutrality in an intrinsic region. Thus, the number of holes in the active region is identical to the number of electrons, and we only need to keep track of the single carrier density (electron).

Now, using what we know about the spontaneous recombination processes and the fact that the carrier density is pinned at and above lasing threshold, we will arrive at the

answer to our second question. At threshold and above, the three spontaneous recombination processes (*defect*, *spontaneous*, and *Auger*) are pinned due to the pinning of the carrier density. *Thus, we must observe carrier lifetimes below threshold in order to obtain carrier lifetimes as a function of current, which ultimately allows us to determine the carrier density in the active region of the laser and extract the A, B and C coefficients of the spontaneous recombination rate equation.* There are several methods used to perform carrier lifetime measurements; however, we will limit our discussion to the one used in this research—the impedance independent optical response technique.

2.4 Impedance Independent Optical Response Technique

The impedance independent optical response technique is a small-signal technique in which a small AC signal is superimposed on a DC bias signal. This technique was first introduced by [7]. It was designed to avoid the challenging experimental setup of the turn-on delay technique [8], and the additional work needed to perform the impedance corrected optical response technique [9]. To adequately introduce the impedance independent optical response technique, we will first examine the experimental setup and its requirements, then we will examine how and why this technique works from the laser rate equations point of view.

Figure 2.6 is an illustration of the experimental setup of the impedance independent optical response technique. The laser is biased through the bias tee network. Upon biasing the laser, a collimating lens is used to capture and collimate the light coming from the laser. Then a focusing lens is used to focus the light onto a PIN photodetector. The signal coming from the photodetector is then amplified through a voltage amplifier before being transmitted to the spectrum analyzer. All of the instruments—the amplifier, lenses, photoreciever circuit,

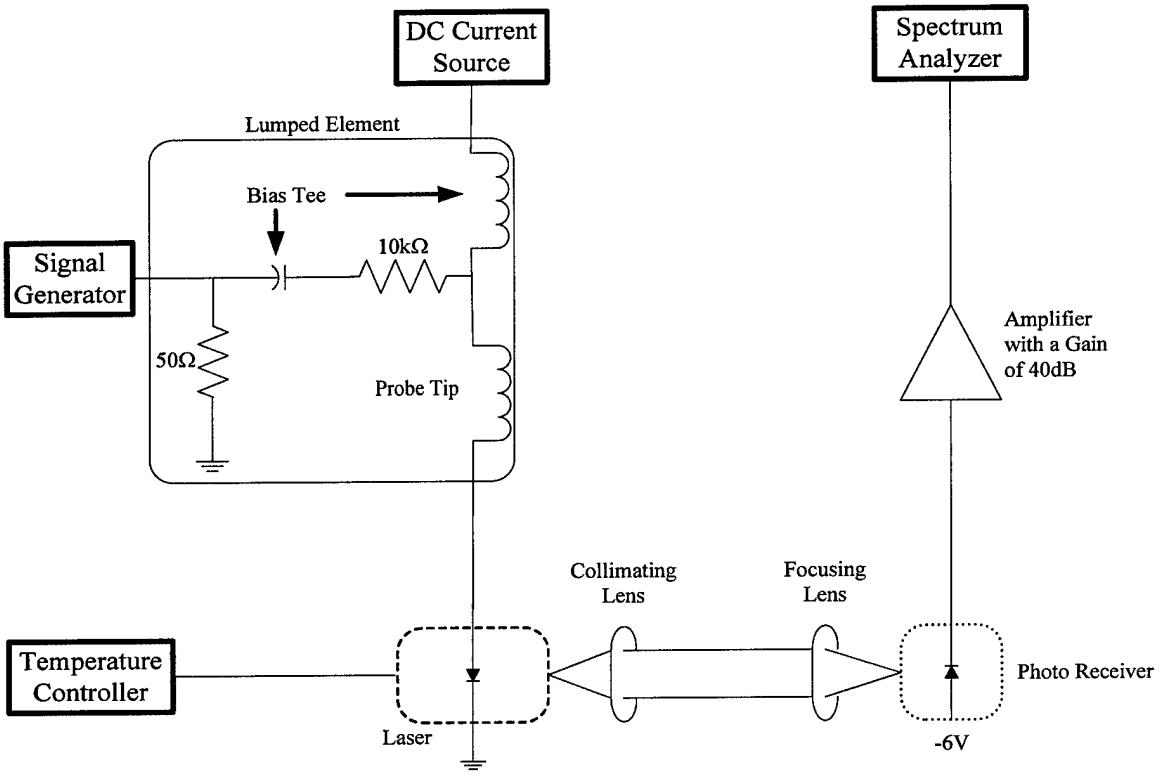

Figure 2.6: Experimental setup for the impedance independent optical response technique. It is used for examining the small-signal response of a semiconductor laser, which ultimately leads to the extraction of differential carrier lifetimes.

and bias tee circuit—are all essential for the experimental setup; however, the validity of the experimental results ultimately rests upon the design of the bias tee circuit. *The sole responsibility of the bias tee circuit is to deliver a* ***constant*** *small-signal modulation current to the semiconductor laser*. The importance of this feature is revealed when we examine the small-signal version of the laser rate equations.

2.4.1 Small-Signal Laser Rate Equations

The impedance independent optical response technique is a small-signal response technique, thus the lifetimes we measure are differential carrier lifetimes [10]. The definition of the differential carrier lifetime is found in eqn 15.

$$\frac{1}{\tau'} = \frac{\partial R}{\partial n} = A + 2Bn + 3Cn^2.$$

Eqn. 16 Differential carrier lifetime definition
Units: sec^{-1}

The small-signal form of the laser rate equations can be pursued one of two ways: taking a differential of each of the laser rate equations; or substituting a constant DC term and a small-signal AC term into the laser rate equations [5]. Both methods will yield the same results, but for intuitive reasons, we will pursue the latter method—substituting the DC and small-signal AC terms. In order to perform this substitution we make the following definitions for the injected current, carrier density and photon density.

$$I = I_o + i_1 e^{j\omega t}$$ **Eqn. 17 Large and small signal injection current**

$$n = N_o + n_1 e^{j\omega t}$$ **Eqn. 18 Large and small signal carrier density**

$$s = S_o + s_1 e^{j\omega t}$$ **Eqn. 19 Large and small signal photon density**

Since we are observing carrier lifetimes below threshold, we need to introduce the below threshold laser rate equations—just the original set of laser rate equations with the stimulated emission terms set to zero.

$$\frac{dn}{dt} = \frac{\eta_i I}{qV} - \frac{n}{\tau}$$ **Eqn. 20 Carrier density rate equation below threshold**

$$\frac{ds}{dt} = \frac{\beta n}{\tau} - \frac{s}{\tau_p}$$ **Eqn. 21 Photon density rate equation below threshold**

If we substitute the large and small-signal equations (16-18) into the below threshold laser rate equations and separate the time dependent terms from the time independent terms, we obtain the following small-signal laser rate equations [6].

$$j\omega n_1 = \frac{\eta_i i_1}{qV} - \frac{n_1}{\tau'}$$ **Eqn. 22 Small-signal carrier density rate equation**

$$j\omega s_1 = \frac{\beta n_1}{\tau'} + \frac{s_1}{\tau_p}$$ **Eqn. 23 Small-signal photon density rate equation**

Experimentally, we observe the small-signal optical response of the laser, so we need to solve for s_1—the small signal photon density term. Solving equations 22 and 23 for the small-signal photon density yields the following equation [6].

$$|s_1| = \frac{\eta_i \beta i_1}{\tau' q V}\left[\frac{1}{\left(\omega^2 + \frac{1}{\tau_p^2}\right)\left(\omega^2 + \frac{1}{\tau'^2}\right)}\right]^{1/2}$$

Eqn. 24 Intermediate equation for the small-signal photon density

Now, if we recognize that the photon lifetime resides at much higher frequencies than the differential carrier lifetime and bring τ' under the square root sign, we can put the small-signal photon density equation in the following form.

$$|s_1| = \frac{\beta i_1 / qV}{\sqrt{1 + \omega^2 \tau'^2}}$$

Eqn. 25 Final small-signal carrier density rate equation

One important observation must be gleaned from this equation in order for us to understand what our experimental results should yield: *the small-signal optical response will be a single-pole response if the amplitude of the small-signal modulation current i_1 remains constant with frequency; this ensures an accurate extraction of the differential carrier lifetime occurs.* Now, we see why it is important to deliver a constant small-signal modulation current to the semiconductor laser. Before we move on to see how the bias tee circuit physically delivers a constant modulation current to the semiconductor laser, we need to consider why we might expect to observe a single-pole response from this experiment.

Physically, the small-signal AC current is pushing carriers into and then pulling carriers out of the laser. Thus, if we push carriers into and out of the laser at a rate much slower than the rate at which these carriers are recombining, we will successfully modulate the light output of the laser. That is, we will successfully raise and lower the light output of the laser because the carriers we initially injected at the beginning of the cycle will have recombined (raising the light output) before we attempt to take them back out. Thus, when we remove carriers in the second half of the cycle we remove carriers delivered by the DC bias signal (reducing the light output). This process of injecting and removing carriers

occurs in this fashion until we begin injecting and removing carriers at a rate equal to or greater than the differential lifetime of the carriers. At this point, we are essentially injecting and removing carriers before they have a chance to spontaneously recombine; therefore, we begin to see less and less of a response from the laser at frequencies beyond where the differential carrier lifetime is observed—this is physically why we see the single-pole response in our experimental results.

2.4.2 The Bias Tee Circuit

Figure 2.7 is a blown up view of the bias tee circuit found in figure 2.6.

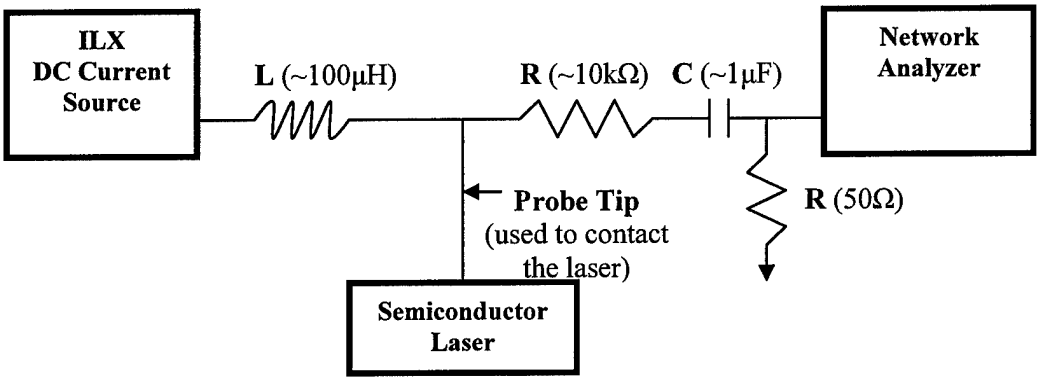

Figure 2.7: Bias tee circuit used in the impedance independent optical response technique.

The DC side of the bias tee consists of an inductive network (illustrated by a single inductor). The inductive network's job is to exhibit a large impedance in comparison to the laser impedance over the frequency range of interest (1MHz to 1GHz). The necessity of this feature is to ensure as much of the small-signal modulation coming from the network analyzer is delivered to the laser and not wasted in the inductive network. The AC side of the bias tee consists of a 50Ω shunt resistor, a capacitor, and a resistive network. The 50Ω shunt resistor is used to make the bias tee circuit and laser look like a matched load to the network analyzer to avoid reflections of the incident signal—a large impedance (everything beyond the 50Ω shunt resistor) in parallel with a 50Ω resistor ensures the impedance looking

into the bias tee is virtually 50Ω. The capacitor used in the AC network is used to block the DC signal from creeping up to the network analyzer. The resistive network is used to maintain a constant modulation current to the laser: the resistive network is to look large in comparison to the laser impedance, thereby ensuring a constant modulation current is delivered to the laser diode regardless of the changing impedance of the laser (it is frequency and bias dependent as we will later see). The final element of the bias tee circuit is the probe tip—its job is to merge and deliver both the DC bias and small AC signal to the semiconductor laser [7].

From this analysis, we see all of the elements are important for the operation of the bias circuit, but it is the resistors and inductors we depend heavily on to maintain a constant modulation current. That is, we would like the inductors to behave as an open circuit when viewed by the AC current to ensure all of the modulation current is delivered to the laser diode, and we would like the resistive network to maintain a large, constant impedance regardless of the operating frequency to ensure that a small signal current, constant in amplitude, is delivered to the laser diode. If we can develop a circuit capable of doing this, we will undoubtedly yield good experimental results. However, this job is not as easy as it looks, for we have not yet considered the high frequency models of the components needed to implement the bias tee circuit design.

2.5 High Frequency Models and the Semiconductor Laser Equivalent Circuit

Figure 2.7 illustrates the ideal circuit elements used to construct the bias circuit; however, at high frequencies we begin to see the parasitic features of these elements reveal themselves. Therefore, this section is dedicated to exposing the parasitic features of each of these elements which are responsible for turning inductors into capacitors, capacitors into inductors, and resistors into capacitors at high frequencies. In addition to this, we will

examine the equivalent circuit for the semiconductor laser in order to shed some light on why the process of constructing the bias tee circuit is a rather difficult process—it stems not only from the parasitic elements of the bias tee circuit components but also from the bias and frequency dependent nature of the semiconductor laser itself.

2.5.1 Equivalent Circuit for a Resistor at High Frequency

The equivalent circuit for a resistor at high frequencies is illustrated in figure 2.8 [11].

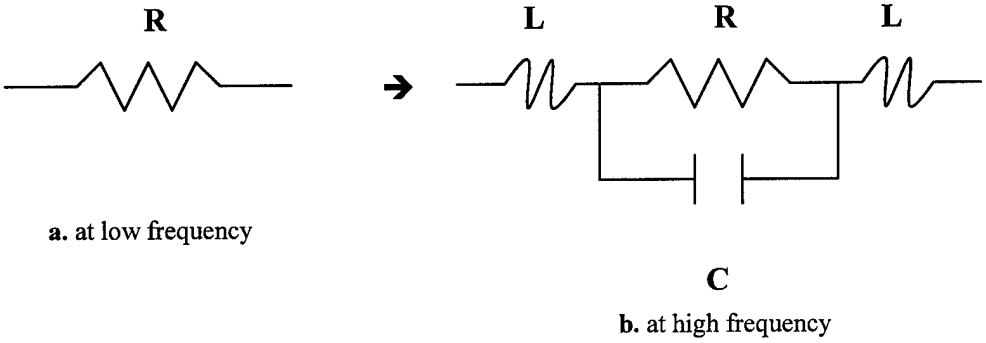

a. at low frequency

b. at high frequency

Figure 2.8: a. resistor at low frequency **b.** high frequency equivalent circuit for a surface mount resistor [11].

The inductances (L) are due to the leads of the component. The resistance (R) is the nominal resistance of the resistor, and the capacitance (C) is due to the substrate material in which the resistive material is placed on [11]. The impedance behavior of a typical surface mount resistor can be observed in figure 2.9.

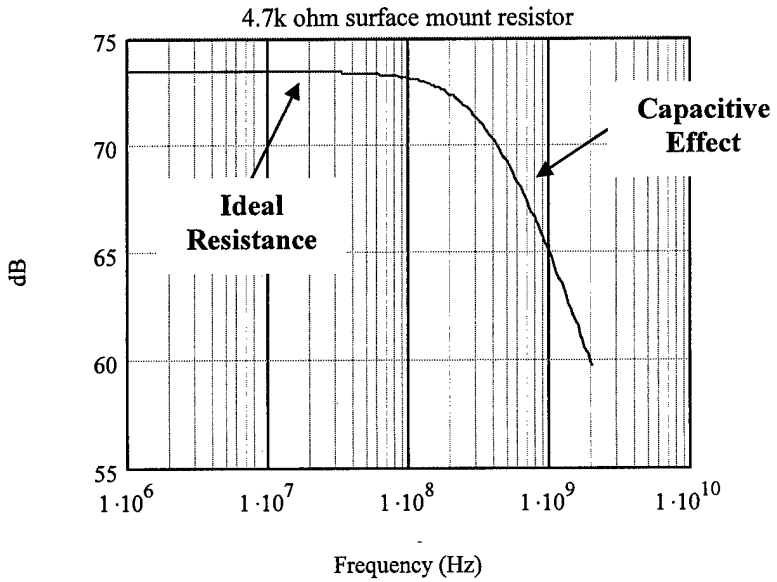

Figure 2.9: Actual impedance data taken on a 4.7kΩ surface mount resistor.

From figure 2.9, we see the surface mount resistor exhibits an ideal resistive behavior at low frequencies. However, at higher frequencies, the impedance offered by the parasitic capacitance begins to decrease below the impedance offered by the resistive material. At this point, the parasitic capacitor begin passing the AC signal rather than forcing the AC signal through the resistor. This capacitive effect generally continues until we reach frequencies where the impedance offered by the parasitic lead inductance becomes significant. At this point, we will begin observing an inductive rise in the impedance. This inductive effect is not seen in figure 2.9 because it is typically not observed below 10GHz [11]. However, as seen from figure 2.9, the parasitic capacitive effects can be observed as early as 100MHz for resistive values of a few kΩ's.

2.5.2 Equivalent Circuit for a Capacitor at High Frequency

The equivalent circuit for a capacitor at high frequencies is illustrated in figure 2.10 [11].

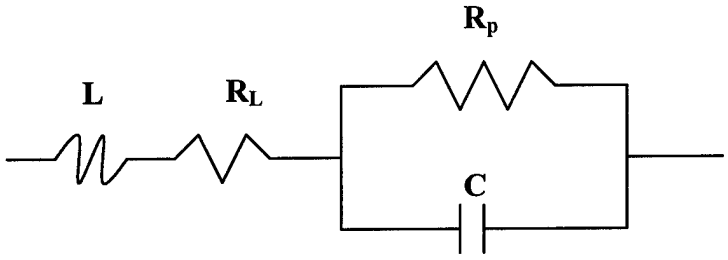

Figure 2.10: Equivalent circuit for a capacitor at high frequencies [11].

The inductance (L) is again due to the lead inductance. The resistance (R_L) is due to the lead resistance. The resistance (R_p) is due to the dielectric material, which is highly resistive and presents losses in the form of heat. Finally, the capacitance (C) is the nominal capacitance of the capacitor [11]. The impedance behavior of a capacitor with its parasitic elements can be observed in figure 2.11.

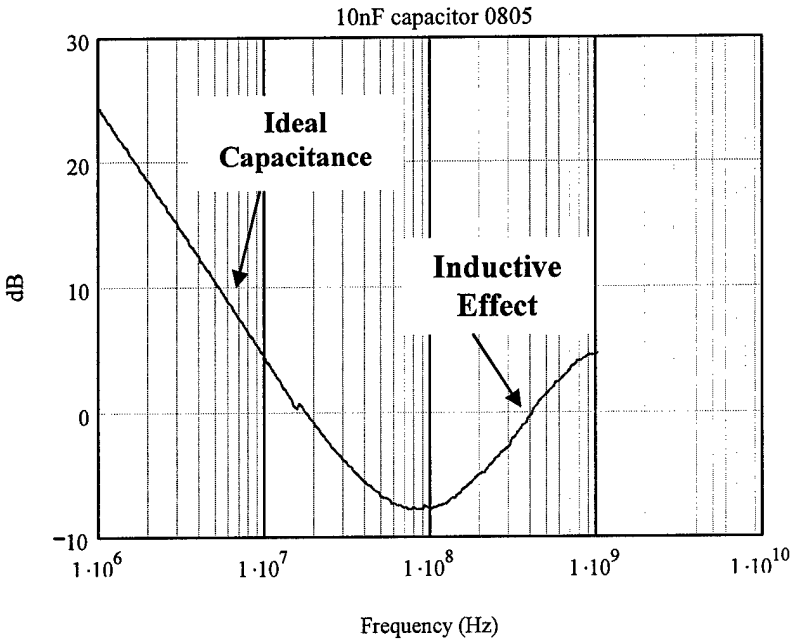

Figure 2.11: Actual impedance data from a 10nF capacitor.

What can be gleaned from figure 2.11 is the capacitor behaves ideally until the frequency of operation approaches the resonant frequency of the capacitor. At this point, the impedance bottoms out at the lead resistance. Following this, the lead inductance takes over, causing the capacitor to behave as an inductor at high frequencies.

2.5.3 Equivalent Circuit for an Inductor at High Frequency

The equivalent circuit for an inductor at high frequencies is illustrated in figure 12 .

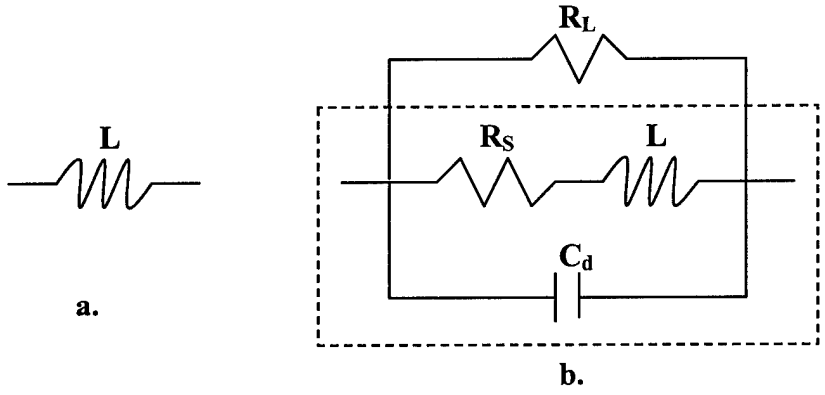

Figure 2.12: a. inductor at low frequency **b.** high frequency equivalent circuit for an inductor at high frequencies—the boxed in portion is the equivalent circuit found in [11,12].

The portion of the high frequency circuit which is boxed-in is the high frequency equivalent circuit found in textbooks [11,12]. However, the entire high frequency equivalent circuit of figure 2.12b. was found to yield a better magnitude and phase impedance fit than the textbook high-frequency equivalent circuit. The resistance R_s, is due to the DC resistance of the wire used to construct the inductor. The inductance (L) is the nominal inductance. The capacitance (C_d) is a distributed capacitance due to the finite capacitance existing between each winding of the inductor. Finally, the resistance (R_L) is a lossy element used to illustrate losses beyond just the skin effect and the DC resistance of the wire used to construct the inductor—we believe it is the result of losses coming from the ferrite material surrounding the inductor's coils.

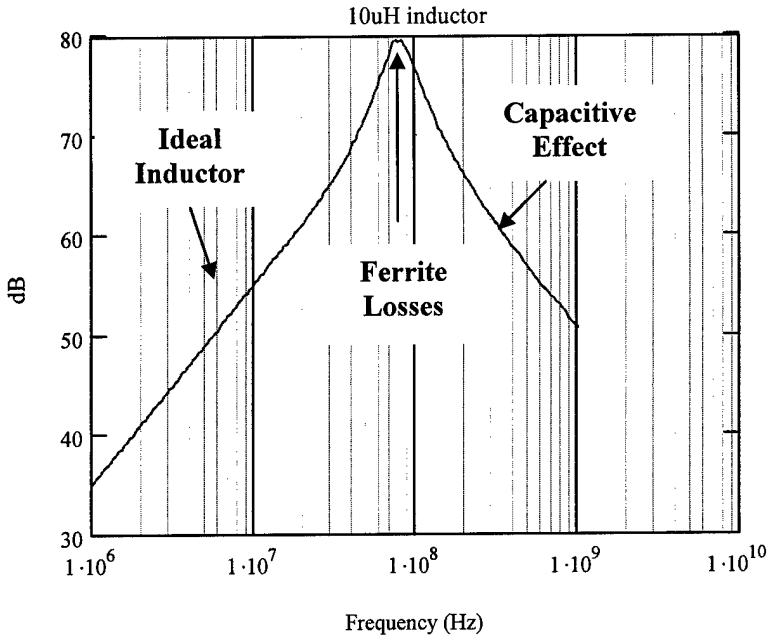

Figure 2.13. Actual impedance data taken on a 10μH inductor.

From figure 2.13, we see the inductor behaves ideally at low frequencies. It behaves inductively until we reach the resonant frequency, where the losses of the ferrite material dominate—this is the behavior predicted from the high frequency inductor model established in figure 12b. Beyond the resonant frequency, it becomes more efficient for the AC signal to

pass through the capacitive network established by the coils of the inductor rather than continue to be lost in the ferrite material. We have now covered the high frequency equivalent circuits for all of the components needed to construct the bias tee circuit except the probe tip inductance.

2.5.4 Equivalent Circuit for the Probe Tip

The high frequency circuit for the probe tip consists of two elements: a resistor and an inductor. The high frequency equivalent circuit for the probe tip is illustrated in figure 2.14.

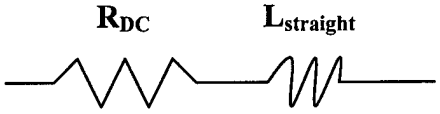

Figure 2.14. High frequency equivalent circuit for the probe tip.

The resistance (R_{DC}) is the DC resistance of the probe tip, and the inductance ($L_{straight}$) is the straight wire inductance given by the following empirical formula, where the radius r and length L are in cm and the inductance is in nH [13].

$$L_{straight} = 2L\left[\ln\left(\frac{2L}{r}\right) - .75\right]$$

Eqn 26. Straight wire inductance empirical eqn.

Thus, if we used a probe tip of length 2mm and radius of 6mils (the approximate dimensions of the probe tip used in our bias tee circuit design), we would obtain an inductance of 1nH—this equates to an impedance of 6.3Ω at 1GHz. Now, we need to examine the equivalent circuit for the laser to see where its bias and frequency dependence stem from.

2.5.5 Equivalent Circuit for Semiconductor Lasers

The small-signal equivalent circuit for semiconductor laser below threshold is illustrated in figure 2.15.

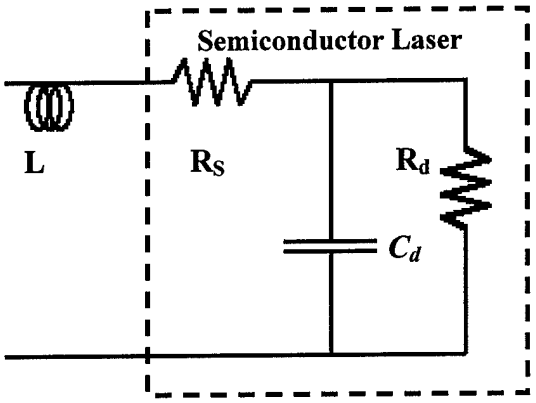

Figure 2.15: Equivalent circuit for a semiconductor laser below threshold [14].

The inductance (L) is due to a parasitic inductance coming from the probe used to bias the laser. The resistance (R_s) is a series resistance stemming from the ohmic contacts on the laser in addition to the P-type and N-type materials in which the carriers must travel through to get to the active region of the laser. The active region is modeled by a differential resistance (R_d), due to the differential resistance of the p-n junction, and it is in parallel with a differential capacitance (C_d), due to the storage of carriers in the active region. Incidentally, R_dC_d is a time constant equivalent to the differential carrier lifetime τ', thus another method of extracting differential carrier lifetimes is through examining the impedance of the laser as a function of current and frequency [14]. We will not discuss the details of this carrier lifetime method, but rather evaluate the below threshold laser impedance derived from the equivalent circuit found in figure 2.15 and point out the bias and frequency dependence.

$$Z_L(\omega) = j\omega L + R_s + \frac{R_d}{1+\omega C_d R_d} = j\omega L + R_s + \frac{R_d}{1+\omega\tau'}$$

Eqn 27. Laser impedance below threshold

Clearly, the laser impedance is frequency dependent stemming from the inductive and capacitive terms present in eqn 27. However, it is also bias dependent due to the differential resistance R_d and differential capacitance C_d. Figure 2.16 illustrates the impedance of a

semiconductor laser as a function of frequency at a low bias of .2mA, and figure 2.17 illustrates the impedance of a quantum well laser as a function of frequency when biased just above threshold at 8mA—laser threshold for this laser was 7mA. Both of these figures illustrate the frequency dependence of a semiconductor laser, where at low frequencies the impedance of the laser is equal to the series resistance plus the differential resistance of the active region. This impedance behavior is maintained until we reach frequencies in which the impedance offered by differential capacitance of the active region decreases below the differential resistance of the active region. At this point, we observe a capacitive trend in the laser impedance until we bottom out at the series resistance of the cladding layers. The difference in the low frequency impedance between the two curves illustrates the bias dependence of the laser impedance, where at lower bias levels the differential resistance of the active region increases. Now, that we have a full view of high frequency behavior of each of the components used in the tee circuit and the behavior of the semiconductor laser with bias and frequency, we are now prepared to look at the design approaches.

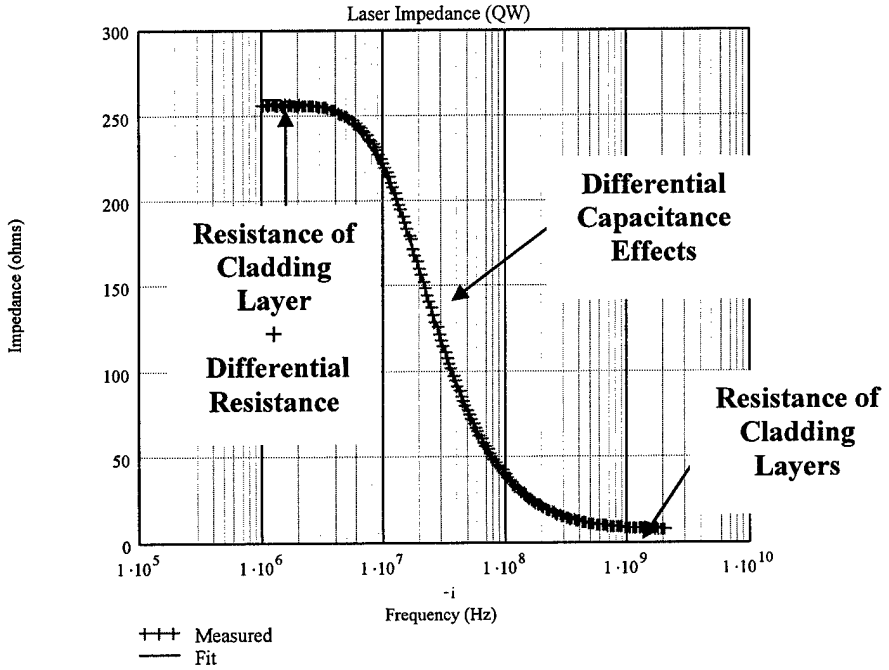

Figure 2.16. QW laser impedance when biased at .2mA.

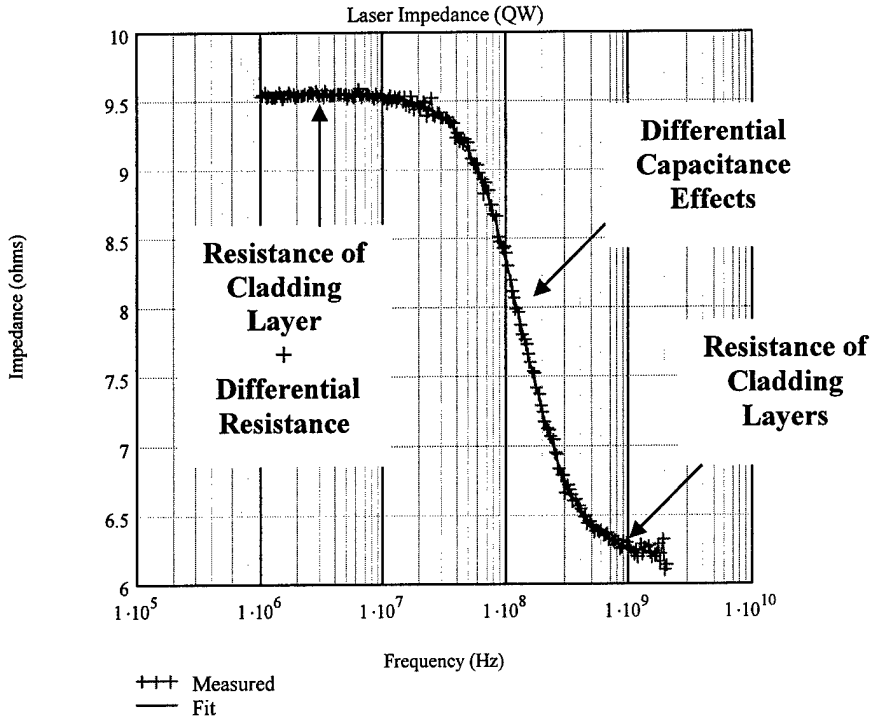

Figure 2.17. QW laser impedance when biased at 8mA.

2.6 Design Approaches

There were two design approaches to developing the bias tee circuit: **1.)** utilize the impedance information found on component data sheets to model the bias tee circuit and model the small-signal laser diode current, **2.)** measure the actual impedance of each component through extracting it from reflection S11 or transmission S21 scattering parameters, then use this information to model the bias tee circuit impedance and the small-signal diode current. The intricate details of the first design approach will be the focus of chapter 3, but what we will see is that the first bias tee circuit design delivered an increasing small-signal modulation current to the laser diode above 200 MHz. For this reason, the second design approach was pursued which is the focus of chapter 4. In this chapter we will see exactly why an increasing modulation current was delivered to the laser diode above 200MHz—an underestimation in the surface mount resistor's parasitic capacitance. We will

also see that two bias circuits must be made: one to obtain differential carrier lifetimes at low bias currents where the impedance of the laser is large, and one to obtain differential carrier lifetimes at higher currents where the impedance of the laser is smaller.

References--Chapter 2

[1] Thyagarajan, K., and Ghatak, A.K., "Lasers Theory and Applications," Plenum Press New York, 1981.

[2] W.W. Chow and S.W. Koch, "Semiconductor Laser Fundamentals: Physics of the Gain Materials," Springer-Verlag Berlin Heidelberg, 1999.

[3] O.B.Shchekin and D.G. Deppe, "1.3μm InAs Quantum Dot Lasers with T_o=161K from 0 to 80°C," Appl. Phys. Lett. Vol. 80, No. 18, 2002: 3277-3279.

[4] J. Pankove, "Optical Processes in Semiconductors," Dover Publications Inc. New York, 1971.

[5] L.A. Coldren, and S.W. Corzine, "Diode Lasers and Photonic Integrated Circuits," John Wiley & Sons, INC., 1995.

[6] J.M. Pikal, "Temperature Dependence of Carrier Lifetime, Recombination, and Gain in 1.3μm InAsP/InGaAsP Multiple Quantum Well Lasers," Dissertation, Aug. 1999.

[7] J.M. Pikal and C.S. Menoni, "Impedance Independent Optical Carrier Lifetime Measurements in Semiconductor Lasers," Review of Scientific Instruments, Vol. 69, No. 12, 4247-4248.

[8] R.W. Dixon and W.B. Joyce, "Generalized Expressions for the Turn-On-Delay in Semiconductor Lasers," J. Appl. Phys., Bol. 50, no.7, pp. 4591-4595, 1979.

[9] G.E. Shtengel, et. al., "Impedance-Corrected Carrier Lifetime Measurements in Semiconductor Lasers," Appl. Phys. Letters, Vol. 67, No. 11, 1506-1508, 1995.

[10] R. Olshansky, et al., "Measurement of Radiative and Nonradiative Recombination Rates in InGaAsP and AlGaAs Light Sources," IEEE JQE, Vol. QE-20, No. 8, Aug 1984.

[11] M.M. Radmanesh, "Radio Frequency and Microwave Electronics," Prentice Hall, 2001.

[12] R. Ludwig, and P. Bretchko, "RF Circuit Design: Theory and Applications," Prentice Hall, 2000.

[13] T. Healy, http://www.ee.scu.edu/eefac/healy/indwire.html. Santa Clara University.

[14] G.E. Shtengel et al. "Advances in Measurements of Physical Parameters of Semiconductor Lasers," International Journal of High Speed Electronics and Systems, Vol. 9, No. 4, 901-940, 1998.

Chapter 3

First Design Approach:

Model and Design Accomplished using Data Sheet Information

3.1 Introduction

This chapter is dedicated to discussing the details of the first design of the bias tee circuit and is divided into 5 sections. The first section is the *Data Sheet Design*: it presents an overview of the design process from start to finish and divides the design into four phases. The second section is *Phase I Gathering Information*: it discusses the parasitic information we gathered from component data sheets and how we handled the situations in which there was no parasitic information to be found. The third section is *Phase II Model*: it describes the MathCad programming that took place to model the small-signal modulation current delivered to the semiconductor laser. The fourth section is *Phase III Design*: it states the components selected for the design and also describes the microwave board layout for the components. The fifth and final section is *Phase IV Testing and Results*: it describes the two experimental tests used to determine if the modulation current delivered to laser diode is constant, and it reveals the results of the design.

3.2 Data Sheet Design

The goal of the first design approach was to perform a data sheet design of the bias tee circuit. The logical flow of the design process is presented in figure 3.1. As with any design process, the data sheet design consists of four phases: gather information (1), model (2-3), design (4), and test (5-6). Each of the design phases has a number of steps—represented by the numbers in parenthesis—before they are considered complete. Thus, we will first briefly discuss the steps presented in figure 3.1, then we will move on to discussing each of the four design phases in detail in sections 3.3 through 3.6.

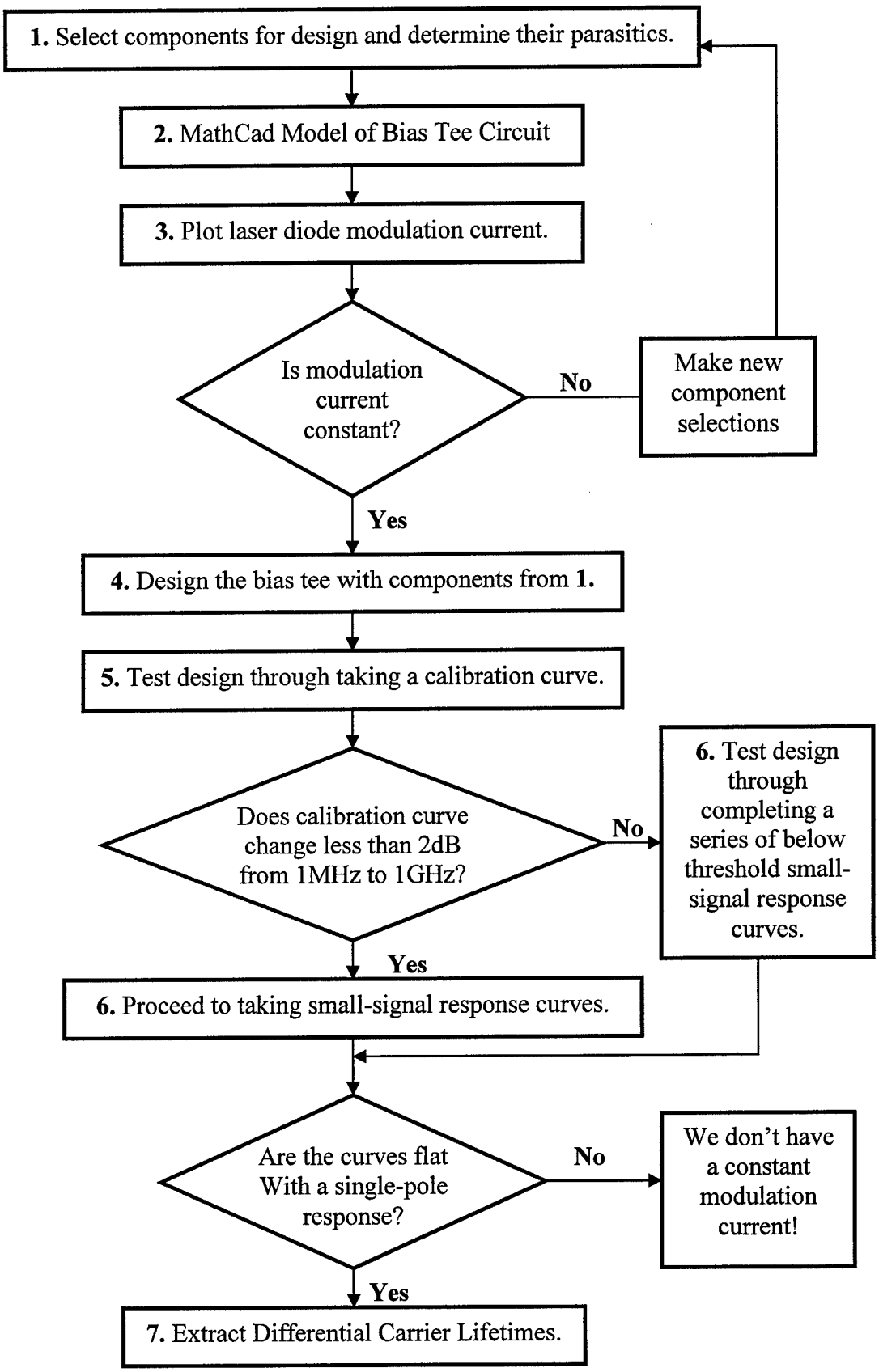

Figure 3.1. Logical flow of the first design approach—the data sheet design.

The logical flow of the data sheet design process begins with making component selections (1) and determining their parasitics, so we can accurately model how the component will behave at high frequencies in the next step—the MathCad model of the bias tee circuit (2). This model is used to take the information gathered on the parasitics of the selected components and model the overall high frequency behavior of the bias tee, allowing us to generate a plot of the laser diode modulation current—step (3). Now, if the plot of the modulation current is not constant from 1MHz to 1GHz, then we make new component selections and run through steps 1 through 3 again, repeating the process until we obtain a constant modulation current for the laser diode from the model.

Once a constant modulation current is achieved from the model, we go to the design—step (4). At this point, we take the components selected in step (1) and generate the bias tee circuit. When this is completed, we move on to the first experimental test of the circuit—taking a calibration curve (5). The intricate details behind the calibration curve test will be revealed in the testing section of this chapter (3.6), but for now we just need to know it is an optical response curve taken of the laser when biased well-above threshold [1,2].

After plotting this curve, we check to see if there is more than 2dB of change in the optical response from 1MHz to 1GHz. If we fall within these limits, we presume a constant modulation current is delivered to the laser and move on to taking below threshold optical response curves (6a). However, if we observe more than 2dB of change in the calibration curve, we do not automatically presume the modulation current to the laser is not constant—there could be systematic errors within the experimental setup the calibration curve is designed to remove (this will make sense later). Instead, we presume there might be nonlinearities within the experimental setup (most of which comes from the amplifier, and some coming from the photodetector, network analyzer, and cable losses), which cause more

than 2dB of change to be observed in the calibration curve. With this said, we move onto another test—taking below threshold optical response curves (6b).

It is true that both steps (6a) and (6b) are identical; however, it is the decision that comes after each of these steps which makes the final call on whether or not we have a valid design. Therefore, we move onto the final decision block. If we observe a nice flat response followed by a single-pole roll-off, we presume we have a constant modulation current whether we are coming from (6a) or (6b). We make this decision based on eqn 24 from chapter 2, which tells us the below threshold optical response is a flat response up to the single-pole roll-off, so long as the modulation current is constant. Now that we have briefly discussed the details of the data sheet design process, we will now move on to describing how each phase of the design was completed starting with gathering information.

3.3 Phase I: Gathering Information

During this phase of the design process, we garnered as much information as possible about the parasitics of resistors, capacitors, and inductors through consulting the manufacturers' data sheets. What we hoped to find on the data sheets were either impedance figures as a function of frequency **or** expected values for the parasitics. However, we were only able to find good impedance figures on the capacitor data sheets and, some, parasitic data on the inductor data sheets. At this stage in the research, we were unable to find parasitic information on the resistors. The following three sub-sections will explain the parasitic information we found on the data sheets and how we dealt with the parasitic information that was not there. Additionally, since we *do* have the actual impedance figures from the measurements taken in chapter 4, we will present figures and compare the modeled impedances with the experimentally measured impedances.

3.3.1 Resistor Data Sheets

Resistor data sheets frequently reveal no figures on the high frequency behavior of their components [3,4]. If figures were present on the resistor data sheets, they came in one of two forms: they only show the high frequency behavior of small resistors [5], which tells you nothing about the parasitic capacitance or lead inductance below ~10GHz; or they display impedance ratio figures [6], which make it more difficult, but possible, for the buyer to extract the parasitics. Although the figures presented by [6] would have been helpful in determining the parasitics of chip resistors at this stage in the research, we did not discover these figures until late in the second design approach—after we experimentally measured the parasitic capacitance and began looking for new resistors. Thus, we had no parasitic capacitance or lead inductance values for resistors at this point in the research.

With no parasitic capacitance or lead inductance values in our grasp, we felt we were safe using two 5.1kΩ resistors (5.0kΩ resistors were not available) to obtain the approximately needed 10kΩ worth of resistance in the bias tee. It never occurred to us that the parasitics of this size of resistor would limit our bandwidth to less than 1GHz; therefore, we made approximations for the parasitics of the resistors such that they would not be observed below 1GHz. We established a parasitic capacitance of .01pF and a lead inductance of .1nH for the 5.1kΩ resistors (figure 2.8 pg 26 illustrates the high frequency model for the resistor). Figure 3.2 compares the experimentally measured (actual) impedance of the 5.1kΩ resistor with the modeled 5.1kΩ resistor impedance.

From this figure, we can see there was a serious underestimation in the parasitic capacitance of the modeled resistor—actually by a full order of magnitude. Also gleaned from this figure is the fact that the parasitic inductance was not seen in either the modeled or the actual impedance curves. Thus, it was not necessary to include them in the model, but it

did not hurt us by including them either. On a final note here, the under-estimation of the parasitic capacitance did help us to attain a constant modulation current in the model; however, the effects of this underestimation show up in the testing and results section.

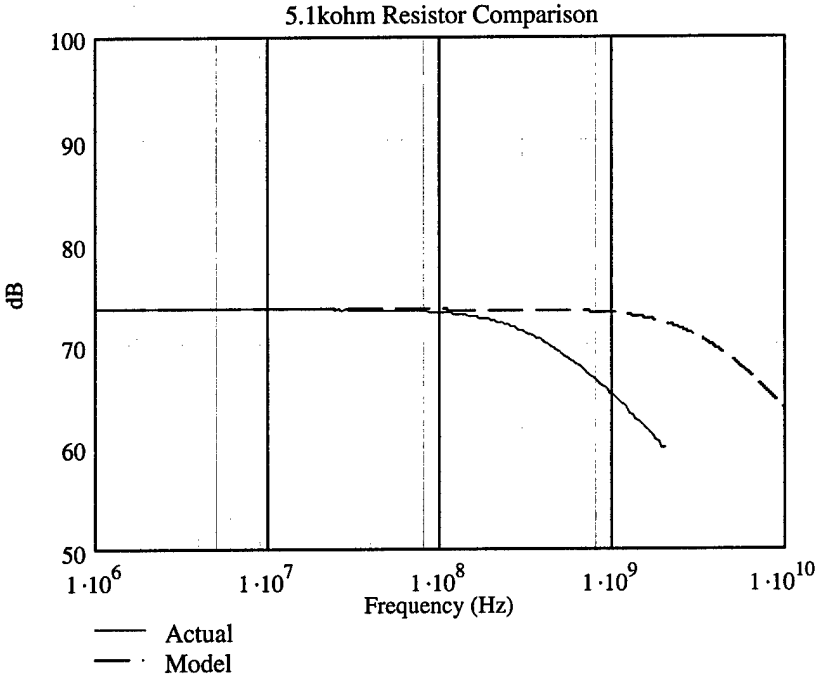

Figure 3.2. Comparison between the actual impedance of the 5.1kΩ resistor and the modeled 5.1kΩ resistor.

3.3.2 Capacitor Data Sheets

As previously mentioned, data sheets illustrating the high frequency behavior of capacitors were readily found [7]. We selected a .1μF capacitor, since it offers very little impedance in the frequency range of interest: according to data sheet [7], it offered ~2Ω of impedance at 1MHz (ideal behavior) and ~10Ω of impedance at 1GHz (stemming from the lead inductance). Since we would like to model this impedance behavior, we extracted the lead inductance and the lead resistance values from the impedance figure in [7]. We obtained 16nH for the lead inductance, and .07Ω for the lead resistance (figure 2.10 pg 27 illustrates

the high frequency model for the capacitor). The following figure compares the experimentally measured impedance of the actual .1μF capacitor with the modeled one.

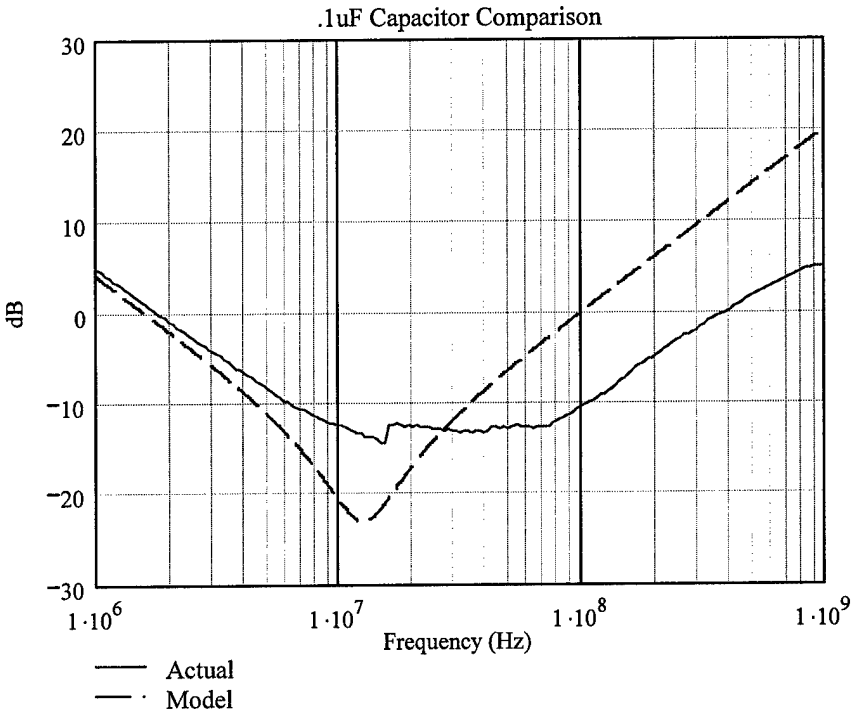

Figure 3.3. Comparison between the actual impedance of the .1μF capacitor and the modeled .1μF capacitor.

From this figure, we can see that the impedance of the modeled capacitor initially follows the actual capacitor's impedance curve, and then follows the same type of inductive trend at higher frequencies. Overall, it is not a great fit; however, the impedance disparities between the modeled capacitor and the actual capacitor are not significant enough to make a real difference in whether or not we obtain a constant modulation current. This is because the maximum impedance offered by the modeled capacitor is 10Ω and the maximum impedance of the actual capacitor is ~2Ω. Neither of these values is even close to the impedance offered by the resistors, thus no significant changes in the modulation current will be observed due to this capacitor. This is precisely what we want—the capacitors are only there to prevent the DC bias signal from creeping up into the AC current source.

3.3.3 Inductor Data Sheets

Inductor data sheets were rather forthcoming with information; they typically showed the DC resistance, self-resonant frequency (SRF), and the quality factor[1] (Q) at a prescribed frequency [8,9,10]. This is sufficient information to retrieve the values of the parasitics for the textbook high frequency model of the inductor [11,12]. Recalling from chapter 2, we need the parasitic resistance and the parasitic capacitance to determine the high frequency behavior of inductors.

If we determine the impedance of the high frequency inductor model (figure 2.12 pg 28) and solve for the resonance condition (imaginary impedance terms cancel), and then solve for the frequency at which this occurs, we will obtain the following definition of the self-resonant frequency of the inductor in terms of the parasitic capacitance (C) and the nominal inductance (L).

$$SRF_{inductor} = \frac{1}{\sqrt{LC}}$$

Eqn 1. Self resonant frequency for an inductor using textbook high frequency model.

From this equation, we can directly solve for the parasitic capacitance: we used 6.8μH and 10μH inductors with parasitic capacitances of .23pF and .26pF respectively. As for the parasitic resistance, it is a function of frequency due to the skin effect. Knowing the Q of the inductor at a prescribed frequency is sufficient for us to solve for the parasitic resistance coming from the skin effect. Normally you would need the length, gauge, and conductivity of the wire used in the inductor to solve for the resistance coming from the skin effect [12]. However, all of these values just return a constant (K) and the resistance coming from the skin effect becomes the following equation [12].

[1] The quality factor is a measure of the ability of an element to store energy equal to 2π times the average energy stored divide by the energy dissipated per cycle [12]. For an inductor $Q=\omega L/R$, thus it is a function of frequency due to the impedance of the inductor and the skin effect.

$$R_{skin}(f) = K\sqrt{f}$$ **Eqn 2: Resistance due to the skin effect**

Thus if we know the value of the parasitic resistance of the inductor at a single frequency, we can solve for the constant K and obtain the expression for $R_{skin}(f)$. In our data sheets, we were given the Q of our inductors at 1MHz; therefore, we were able to solve for $R_{skin}(1MHz)$ and the K values of our inductors. The values for K were .001124 and .001653 for the 6.8μH and 10μH inductors respectively. With these values in-hand, we have all the data needed for the high frequency model of the inductor. Figure 3.4 illustrates the high frequency behavior of our modeled 10μH inductor and the actual behavior of the inductor.

From this figure, we can see that the modeled impedance curve matches the actual impedance curve nicely until we reach the resonant condition. The sharp peak of the model illustrates an over estimation of the Q of the inductor despite our inclusion of the skin effect—clearly there are actual losses which are not accounted for in the textbook model that serve to reduce the Q of this inductor.

Despite the resonant peak mismatch, it will not adversely affect the modeled modulation current. That is, using the textbook high frequency model of the inductor does not hurt us in this instance—it will not yield a more constant modulation current in our model than we will observe in reality. It is fortunate in this instance because the mismatch occurs in the frequency regime where the impedance of the inductor is much greater than the impedance of the laser. Thus, increasing the impedance even further (the way the modeled inductor does) in this regime will not yield a more constant modulation current delivery to the laser diode. For this reason, we can say that the model for the inductors is not perfect, but it is sufficient to yield consistency between the modeled and experimental results. Now that we have seen how the parasitic information of each of the components to be used in the bias tee circuit were retrieved, it is now time to examine how they were used in the model, and

most importantly how the laser diode modulation current looks after selecting these components

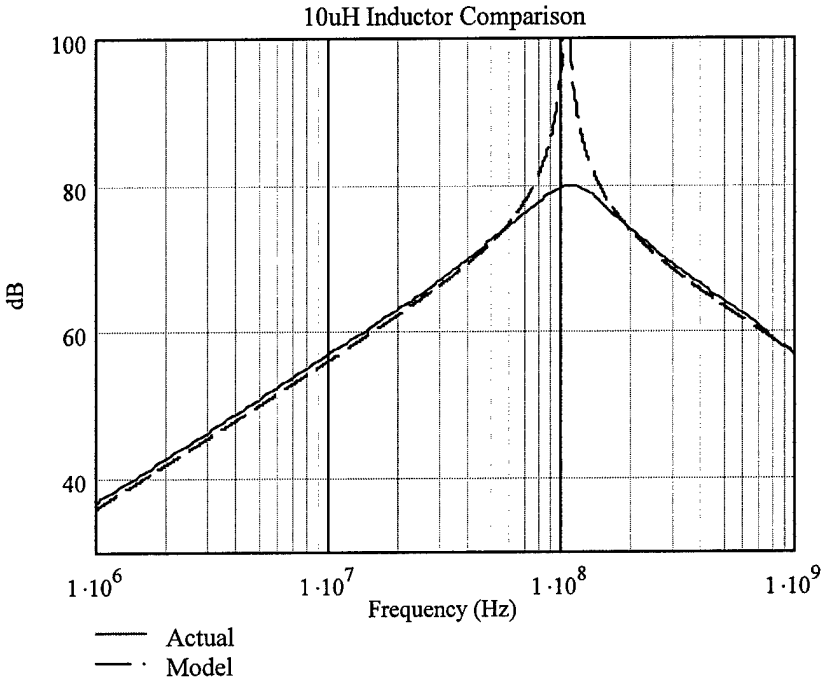

Figure 3.4. Comparison between the actual impedance of the 10μH inductor and the modeled 10μH inductor.

3.4 Phase II: Model

For this phase of the design process, we developed a MathCad program capable of modeling the small-signal modulation current of the laser diode as a function of frequency. The full flow chart for the MathCad program used to model the modulation current and the program itself can be seen in Appendix A. The components used in the model and thus the ones responsible for delivering a constant laser diode modulation current in the model can be seen in table 1. The plot of the modeled modulation current delivered by these components can be seen in figure 3.5.

Component	Dimensions	Size	Parasitics	# used
Resistor	0603	5.1kΩ	$C_p = .01pF$ $L_p = .1nH$	2
Capacitor	0603	.1μF	$L_p = 16nH$ $R_p = .07\Omega$	1
Inductor	1210	6.8μH	$C_p = .23pF$ $R(f) = .001124\sqrt{f}\ \Omega$	1
		10μH	$C_p = .26pF$ $R(f) = .001653\sqrt{f}\ \Omega$	3

Table 3.1. Components with associated parasitics used in the first bias tee circuit design.

From table 3.1, we can see a number of components went into the design in order to obtain a constant modulation current. More inductors could have been used to try and bring down the hump in the modulation current seen in figure 3.5 in the 1MHz to 2MHz regime, but it would have taken several more inductors to do so. Therefore, we used just enough inductors to bring the amount of change in the modulation current down to within 1dB. We did this for two reasons: we were not certain the level of accuracy of the model, and we needed to keep the overall circuit design small, so it could be treated as a lumped element[2].

Getting back to figure 3.5, the laser diode modulation current plot is rather constant with frequency, other than the low frequency hump between 1MHz and 2MHz. This plot was taken with the differential laser diode resistance at 250Ω—used to reflect a laser at low bias. This is considered the most critical area to test our inductive network (under low bias conditions when the laser diode impedance is large), for if the impedance coming from the inductors is not large enough at low frequencies, some of the modulation current will be lost in the inductive network rather than forced into the laser diode. However, based upon the plot, our inductive network seemed to be strong enough since we obtained a constant

[2] A lumped element is a self-contained element that offers on particular electrical property throughout the frequency range in which it is observed. As opposed to a distributed element which is an element whose property is spread out over the length or area of the circuit [13].

modulation current under the low bias conditions. Thus, we are now ready to enter the actual bias tee design phase.

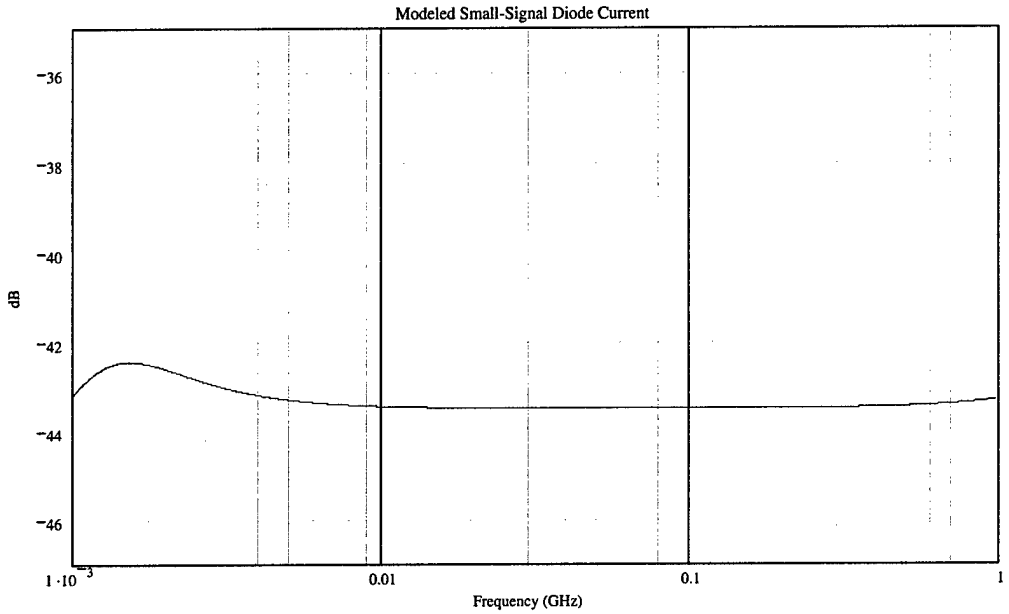

Figure 3.5. The modeled laser diode modulation current at low bias—differential resistance of the laser is 250Ω.

3.5 Phase III Design

During this phase of the design process, we developed a microwave board layout for the bias tee circuit and determined the component placement. The board layout can be found in figure 3.6, and the order of the component placement can be found in figure 3.7.

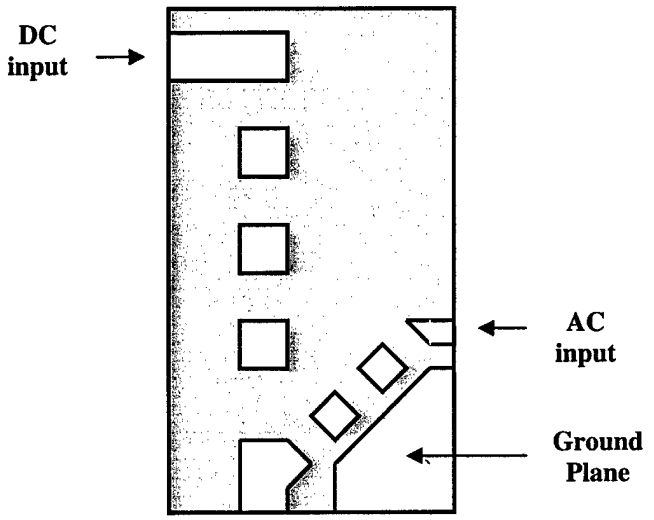

Figure 3.6. Microwave board layout of the bias tee circuit.

The goal of the microwave board design was to make it as compact as possible, leaving just enough room between components for soldering. The external dimensions of the microwave board were 30mm by 20mm. The width of the DC transmission line and pads were 2.0mm and the width of the AC transmission lines were 1.3mm—to obtain a characteristic impedance of 50Ω. Through examining figure 3.7 and referring back to figure 3.6, we can see where each of the components resides on the microwave board. As for the probe tip, it is soldered to the pad centered at the bottom of the microwave board.

Once the microwave board was designed and the bias tee components were in place, we placed the circuit in a brass box: a small hole was drilled (~.2mm) in the front of the box to allow the probe tip to extend beyond the box far enough to make contact with the semiconductor laser. We fully enclosed the circuit in a brass box to reduce the cross-talk between the bias circuit and the receiving circuit. This is particularly important when single-pole, optical response of the laser resides at high frequencies (where the cross-talk power is most significant); the optical power of the single-pole response declines at high frequencies, which decreases the signal to noise ratio of the optical response detected in this regime. Once the bias tee circuit and the brass box were constructed, we began testing our modeled design.

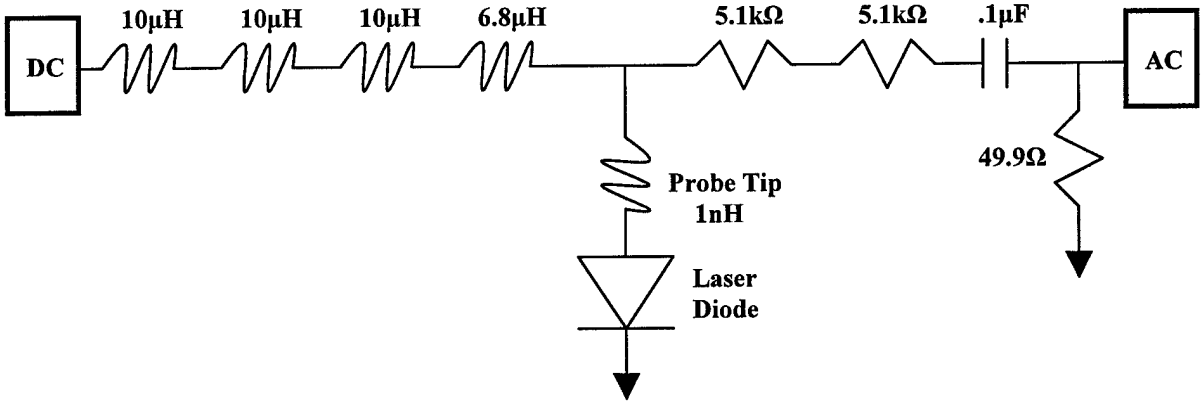

Figure 3.7. First design of the bias tee circuit.

3.6 Phase IV: Testing and Results

Recalling from figure 3.1, the first test of the design is conducted through taking a calibration curve—an optical response curve taken of the laser when it is biased well above threshold [2,13]. Now, the calibration curve performs one very large job for us—it captures all of the systematic errors present in the experimental setup stemming from nonlinearities in the modulation current source, photodiode, cables, and amplifier [2,13]. This is very important because if we can capture the systematic errors of the experimental setup, we can effectively remove them from the below threshold optical response data: we do this by subtracting the calibration curve from each of the below threshold optical response curves.

In order for the calibration to perform its job well, it requires two things: we must bias the laser well-above threshold to push the resonant peak (stemming from the above threshold carrier dynamics) high enough in frequency that it will not be observed below 1GHz [1,2,13], and we must have a constant modulation current delivered to the laser over the entire frequency range of 1MHz to 1GHz [1,2]. These two requirements ensure that the calibration curve will only capture the systematic errors of the experimental setup, for if the two above-mentioned requirements are met, the optical response of the laser will be absolutely flat. Thus anything other than a flat response is coming from systematic errors inherent to the experimental setup [1,2].

We expect the systematic errors to introduce less than 2dB of "wiggle" in the calibration curve, and we establish this value as the level of acceptable change in the calibration curve. Any wiggle outside of 2dB, and we begin questioning where it is coming from: we generally suspect the modulation current is not constant, or the amplifier nonlinearities are the cause. However, if we find no clear evidence as to where the additional wiggle is coming from, we move onto taking below threshold optical response data. If the

below threshold response data resembles nice, flat single-pole responses, we have reason to believe the modulation current delivered to the laser is constant (eqn 24 of chapter 2), and the calibration curve is working properly.

At this point, we have discussed both methods of testing the design of the bias tee circuit: the calibration curve, and the below threshold response curves. Thus, we will now turn our attention to the results of these two tests and examine why we decided to take a new approach to designing the bias tee circuit.

Figure 3.8 illustrates the calibration curve taken using the first bias tee circuit design. From this figure, we see the power of the optical response remains relatively constant from 1MHz up to ~40MHz. Following this, the power decreases ~4dB by the time it reaches 200MHz. Then, from 200MHz to 1GHz, the power of the optical response increases dramatically—nearly 12dB. These results clearly fall outside the acceptable 2dB range, thus we immediately began searching for answers.

We started by examining the magnitude response of the HP amplifier we were using. The response curve of the amplifier can be seen in figure 3.9. There are some similarities between the two curves. They both have a dip in the 40MHz to 200MHz regime (~4dB in the calibration curve and ~1.4dB in the amplifier response curve), and both increase from 200MHz to 700MHz (~6dB in the calibration curve and ~1.4dB in the amplifier response curve). However, the general trends seen in both curves disappear beyond 700MHz (the calibration curve continues to increase while the amplifier response declines).

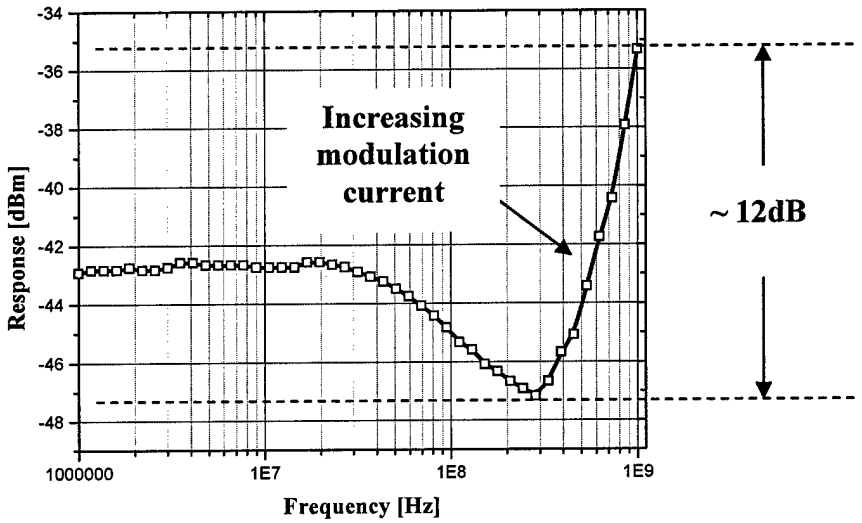

Figure 3.8. Calibration curve from the first bias tee design from 1MHz to 1GHz.

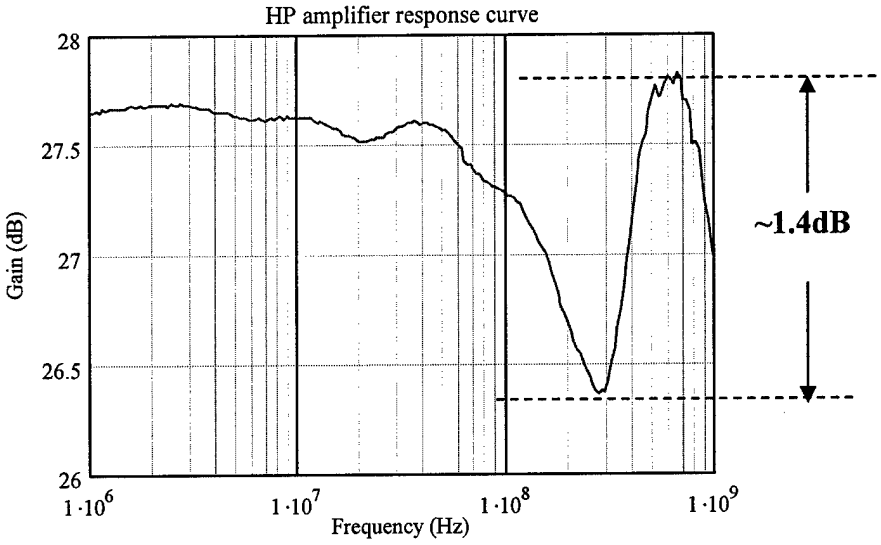

Figure 3.9. Magnitude response of the HP amplifier
from 1MHz to 1GHz

Although there were similar trends between the calibration curve and the amplifier response curve between 1MHz and 700MHz, the amount of change seen in the calibration curve was always much greater than the changes seen in the amplifier response curve. In addition to these disparities, we were concerned with the behavior of the calibration curve beyond 700MHz, as it seemed to be rising quite rapidly while the response of the amplifier

was declining. For these reasons we did two things: we went ahead with taking below threshold optical response curves, and we began working on a new design approach to the bias tee circuit—an experimental approach to designing the bias tee and modeling the modulation current delivered to the laser. The below threshold optical response curves we took were flat with a single-pole response. Two such curves taken by [16] can be seen in figure 3.10. Despite this success, we were still interested in pursuing the second design approach in order to understand the behavior of the calibration curve of figure 3.8. Thus, chapter 4 will discuss the new design approach and reveal why we observe an increasing optical response above 200MHz for reasons other than just the response of our amplifier.

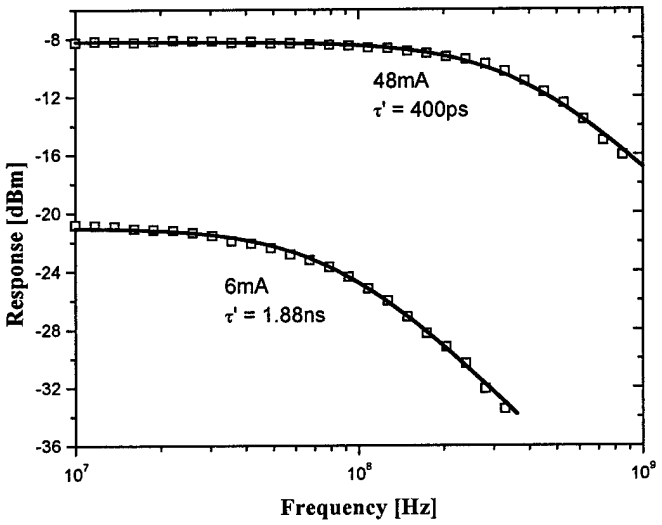

Figure 9. Below threshold optical response curves.

References--Chapter 3

[1] J.M. Pikal and C.S. Menoni, "Impedance Independent Optical Carrier Lifetime Measurements in Semiconductor Lasers," Review of Scientific Instruments, Vol. 69, No. 12, 4247-4248.

[2] J.M. Pikal, "Temperature Dependence of Carrier Lifetime, Recombination, and Gain in 1.3μm InAsP/InGaAsP Multiple Quantum Well Lasers," Dissertation, Aug. 1999.

[3] Panasonic Resistor Data Sheet, "Metal Film Chip Resistors, Rectangular Type 0603, 0805, 1206, 1210, 2512: Type ERA 3Y, 6Y, 8Y, 14, 1W."

[4] Bourns Resistor Data Sheet, "CR0603/CR0805/CR1206-Chip Resistors," http://bourns.com/2/pdfs/CHPREZTR.pdf.

[5] IMS Resistor Data Sheet, "Partial Wraparound Thick Film Chip Resistors for High Frequency Applications," http://www.ims-resistors.com/RCX%20Partial%20Wrap.pdf.

[6] Vishay Resistor Data Sheet, "Thick Film, Rectangular Chip Resistors: D...-CRCW"

[7] Panasonic Capacitor Data Sheet, "Multilayer Ceramic Capacitors for General Series ECJ."

[8] J.W. Miller Inductor Data Sheet, "Shielded Chip Inductor: PM1008S Series."

[9] API Delevan, "Shielded Surface Mount Inductors: Series S1812."

[10] AOBA Technology Co., "SWI 1008 Series Wire Wound Chip Inductors."

[11] R. Ludwig, and P. Bretchko, "RF Circuit Design Theory and Applications," Prentice Hall, 2000.

[12] M.M Radmanesh, "Radio Frequency and Microwave Electronics," Prentice Hall, 2001.

[13] L.A. Coldren, and S.W. Corzine, "Diode Lasers and Photonic Integrated Circuits," John Wiley & Sons, INC., 1995.

Chapter 4

Second Design Approach:

Model and Design Accomplished Using Experimentally Measured Impedances

4.1 Introduction

This chapter is dedicated to discussing the details of the second design of the bias tee circuit and is divided into 5 sections. The first section is the *Experimental Impedance Measurement Design*: it presents an overview of the design process from start to finish. The second section is *Phase I Gathering Information*: it discusses how we gathered the impedance information and why we chose to use S21 (forward transmission coefficient) measurements instead of S11 (input reflection coefficient) measurements to obtain the impedance of our components. The third section is *Phase II Model*: it describes the MathCad programming that took place to model the small-signal modulation current delivered to the semiconductor laser. The fourth section is *Phase III Design*: it states the components selected for the design and the microwave board layout. The fifth section is *Phase IV Testing and Results*: it describes the experimental results of both bias tee circuit designs and an improvement which could help obtain more accurate carrier lifetime data.

4.2 Experimental Impedance Measurement Design

The goal of this design approach was to conduct experimental impedance measurements on each of the components used in the bias tee circuit. This is done in order to provide accurate details on the impedance behavior of each and every component used in the bias tee circuit—the results of such a comprehensive approach is aimed at providing a more accurate model of the modulation current delivered to the laser diode. The logical flow of the design process is very similar to the one seen in chapter 3 and is illustrated in Figure 4.1.

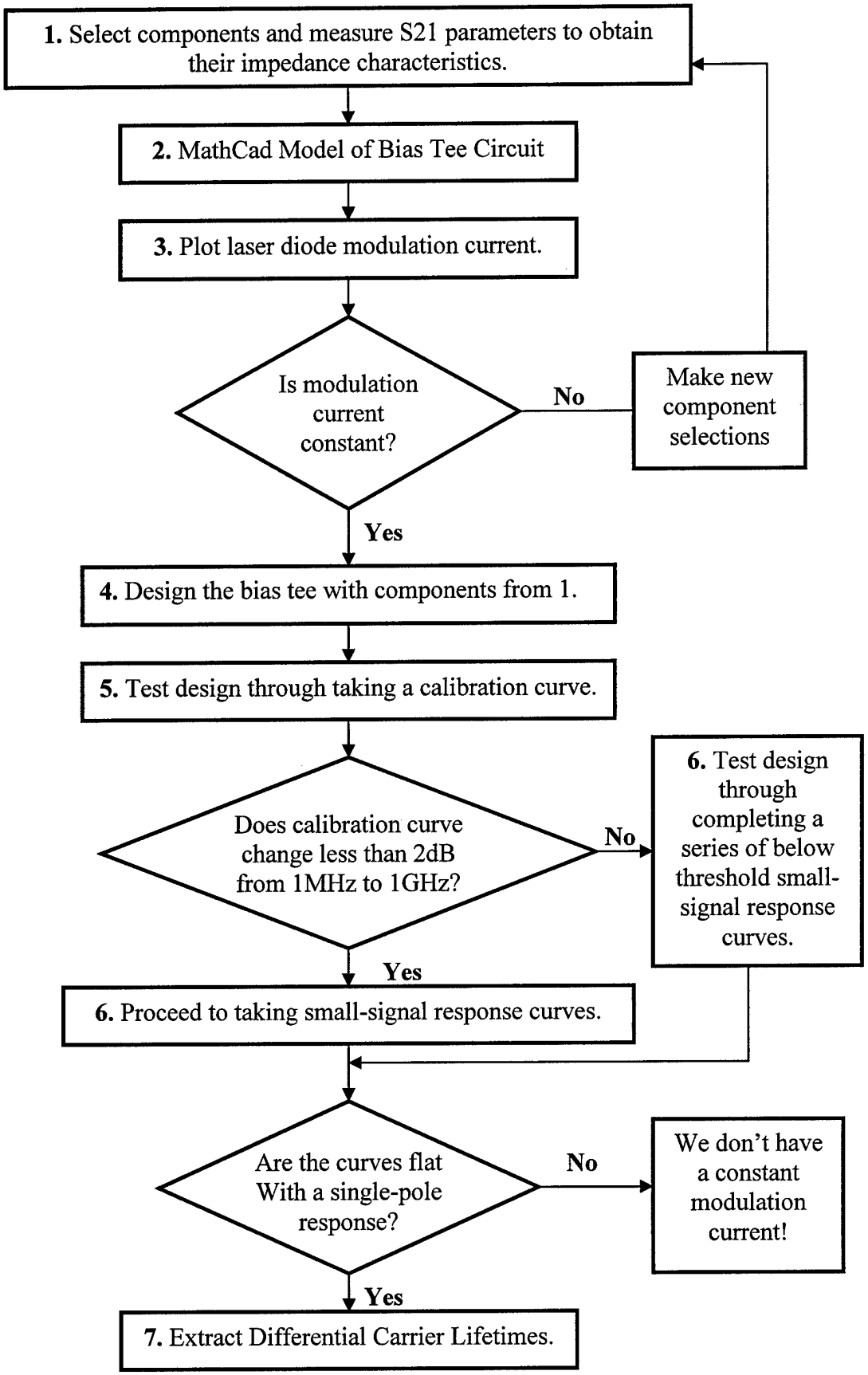

Figure 4.1. Logical flow of the second design approach–the experimentally measured impedance design.

The logical flow of the experimentally measured impedance design begins with making component selections and measuring the S21 parameters of each component through using a network analyzer (step 1). Once we have the S21 parameters of each of the selected components, they are placed in a MathCad model (step 2) designed to convert the S21 parameters into the actual impedance behavior of the components, enabling us to model the overall impedance behavior of the bias tee circuit and generate a plot of the laser diode modulation current (step 3). Now, if the plot of the modulation current is not constant from 1MHz to 1GHz, then we make new component selections and run through steps 1 through 3 again, repeating the process until we obtain a constant modulation current for the laser diode from the model. At this point, we can see the design approach only differs from the first design in one way—the method in which we obtain the impedance of each component. Thus, we will begin examining the four design phases (gathering information, model, design, test and results).

4.3 Phase I: Gathering Information

During this phase of the design process, we initially began measuring S11 parameters to obtain the high frequency impedance behavior of our components; however, it was found that these measurements did not yield self-resonant frequencies (SRFs) in-line with the SRFs quoted on the inductor data sheets—the measured SRFs were lower. For this reason, we began measuring the S21 parameters of each of the components.

Measuring the S21 parameters yielded SRFs in-line with the values quoted on the inductor data sheets; they were virtually identical. The reason the SRFs were lower in the S11 measurements is not fully understood; however, it does seem that the lower SRFs stem from an increased parasitic capacitance associated with the S11 measurement technique, which is not present in the S21 measurement technique. Plots illustrating the impedance

disparities between the S11 and S21 measurement techniques are illustrated in figures 4.2 and 4.3.

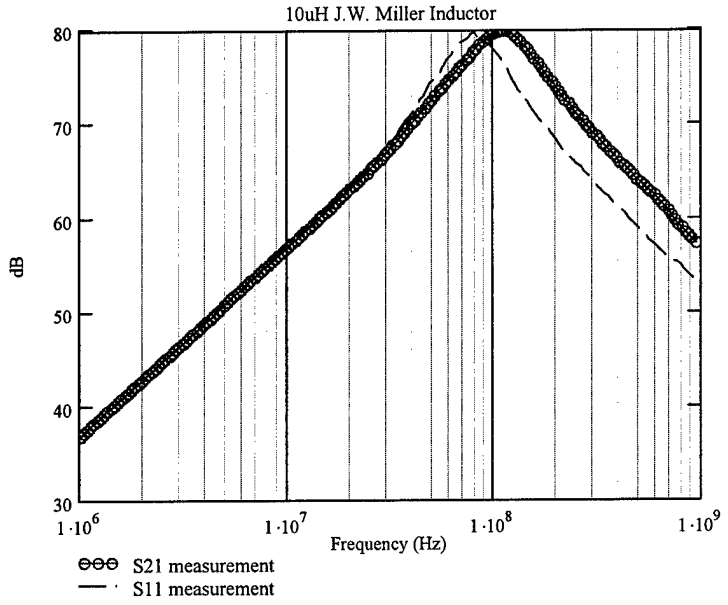

Figure 4.2. Impedance disparities between the S21 and S11 measurement techniques on a 10uH inductor.

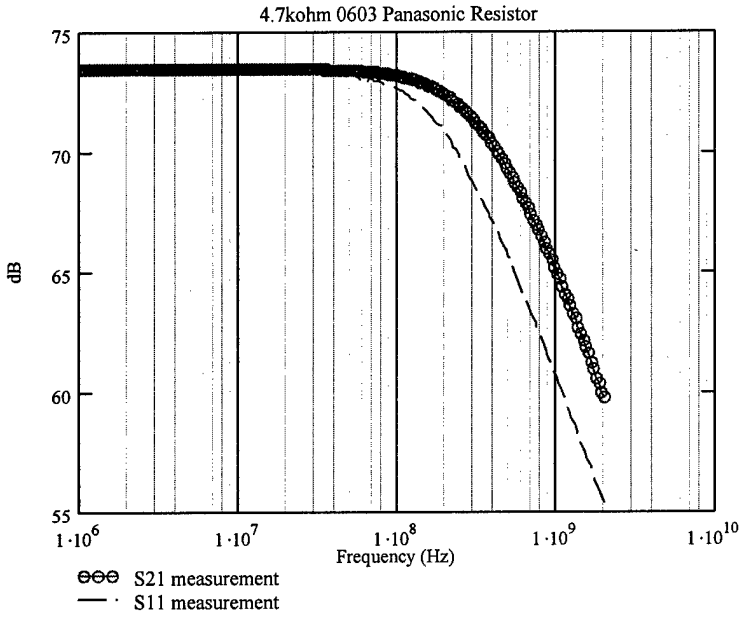

Figure 4.3. Impedance disparities between the S21 and S11 measurement techniques on a 4.7kΩ resistor.

At this point, we need to examine how measuring the S11 and S21 parameters yields access to the impedance of the tested components. Equations 1 and 2 are the definitions of

S11 and S21 parameters, where Z_L and Z_o are the load and characteristic impedances respectively [1].

$$S11 = \frac{Z_L - Z_o}{Z_L + Z_o}$$

Eqn1. Input reflection coefficient definition.

$$S21 = \frac{2Z_o}{Z_L + 2Z_o}$$

Eqn2. Forward transmission coefficient definition.

Clearly, we can solve each of these equations for the load impedance (the impedance of the component we are testing) to obtain the load impedance as a function S11 or S21. This yields the following load impedance definitions from using either S11 or S21 measurements.

$$Z_L = Z_o \frac{1 + S11}{1 - S11}$$

Eqn3. Load impedance as a function of the input reflection coefficient.

$$Z_L = Z_o \frac{2(1 - S21)}{S21}$$

Eqn4. Load impedance as a function of the forward transmission coefficient.

The layout of the microwave board used to conduct the S11 and S21 measurements is illustrated in figure 4.4.

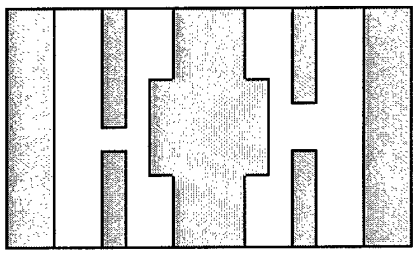

Figure 4.4. Microwave board layout for S21 and S11 measurements.

This microwave board is designed to accommodate 0805 (80 mils by 50 mils) to 0402 (40 mils by 20 mils) components as illustrated by the different, sized gaps in the transmission lines. As for the extra ground plane near the gaps in the transmission lines, these are used for conducting the necessary short and open terminations needed in the calibration procedures. Now we turn our attention to the results of these measurements.

4.3.1 Resistor Impedance

We conducted S21 measurements on resistors with physical sizes of 0402 to 0805 and electrical resistances from 430Ω to 6.7kΩ in order to obtain a sufficiently large data set to make resistor selections for the bias tee circuit. Figure 4.5 illustrates the high frequency impedance behavior of a 3.3kΩ resistor.

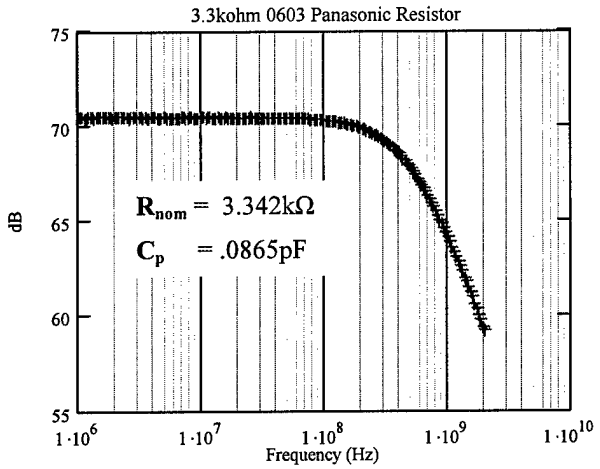

Figure 4.5. Measured impedance of 3.3kΩ 0603 Panasonic resistor.

After reviewing the impedance behavior of the resistor in figure 4.3, it became clear why our modulation current was increasing in our first design—the impedance of our resistors were declining while the input power from the network analyzer remains constant. It was at this point that we decided to design two bias tee circuits: *one used at low bias levels where the impedance of the laser is large and the single-pole, small-signal optical response resides at lower frequencies (~1MHz to ~100MHz); and one used at higher bias levels where the impedance of the laser is low and the single-pole, small-signal optical response resides at higher frequencies (~100MHz to ~1GHz).* Breaking the design into two different bias circuits gives us added flexibility in the design: we take advantage of the laser's low impedance at high biases to get around the low bandwidth problem associated with our resistors.

From this point on, we refer to the two bias circuits as the *low frequency bias circuit* and the *high frequency bias circuit*. The only difference between the two bias circuits is the value of the resistors used—the low frequency bias circuit has two large resistors (each 3.3kΩ) and the high frequency circuit has two small resistors (each 430Ω). For completeness, we present the impedance behavior of the 430Ω resistor used in the high frequency circuit in figure 4.6 and point out the fact that this resistor possesses a higher bandwidth than the 3.3kΩ resistor.

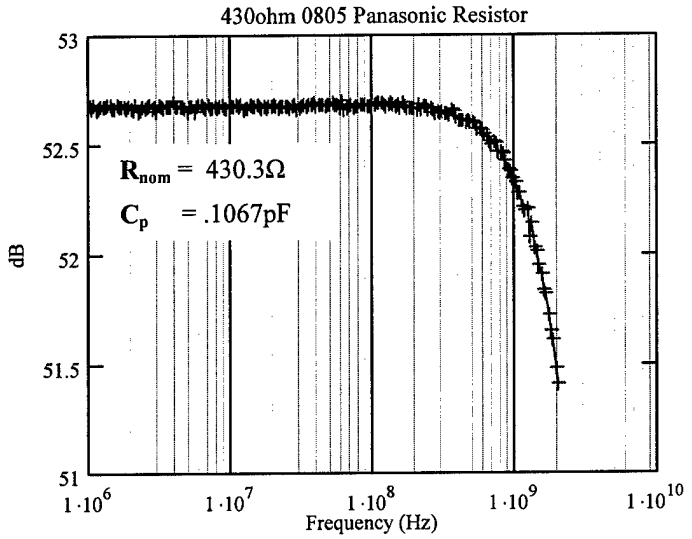

Figure 4.6. Measured impedance of 430Ω 0805 Panasonic resistor—S21 measurement technique.

4.3.2 Capacitor Impedance

Again, we conducted S21 measurements on capacitors with physical sizes of 0402 to 0805 and capacitance values from 10nF to 1μF. Figure 4.7 illustrates the impedance behavior of the .1μF capacitor used in both bias circuits. Although the capacitor impedance does not look well-behaved, the actual impedance offered by this capacitor is small over the frequency range of interest and yields no problems in the modeled modulation current.

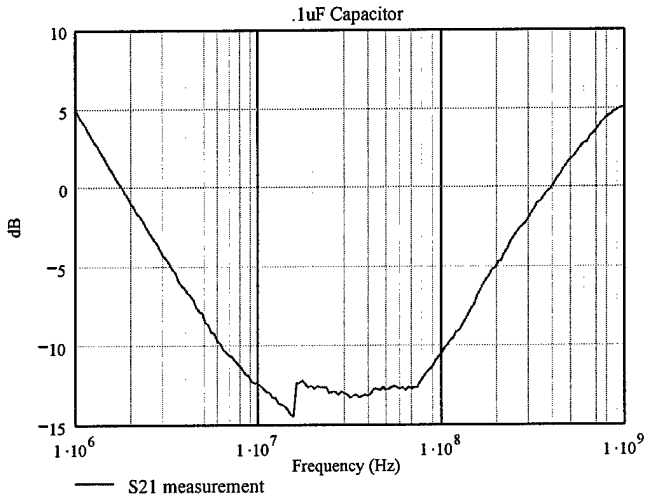

Figure 4.7. .1μF 0603 capacitor impedance data—S21 measurement.

4.3.3 Inductor Impedance

We conducted S21 measurements on inductors with a physical size of 1206 (120 mils by 60 mils) and inductive values from 1000μH to 1.5μH. We selected one 100μH and three 10μH inductors for the bias tee circuits. Their impedance behavior is illustrated in figure 4.8.

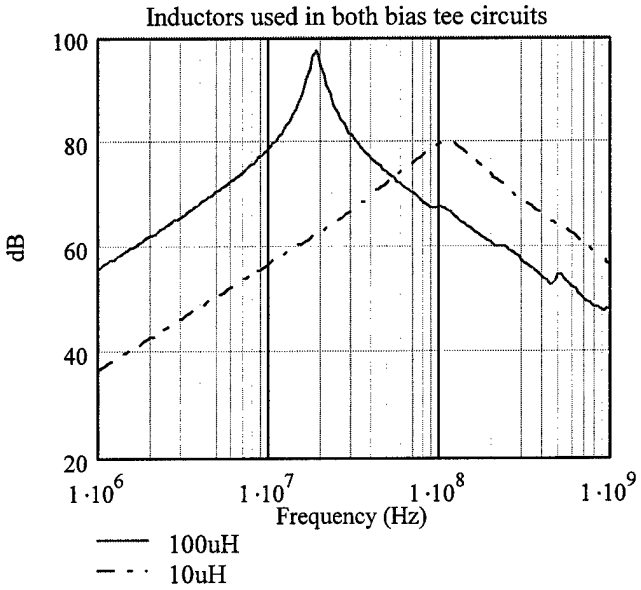

Figure 4.8. Impedance data on the two inductors used in both bias circuits—S21 measurements.

We used a 100μH inductor to increase the impedance of the inductive network at lower frequencies, and three 10uH inductors to maintain a high impedance of the inductive

network in the mid frequencies to high frequencies. The impedance offered by these inductors was sufficient to provide a constant modulation current to the semiconductor laser even at low bias levels when the impedance of the laser is large and the impedance of the inductive network is most critical.

4.3.4 Quantum Dot Laser Impedance

Two members of our research group are conducting carrier lifetime measurements using the impedance technique [2]. They performed S11 measurements on a 27μm wide quantum dot (QD) semiconductor laser at a variety of bias levels, so we could use actual laser impedance in our model. A plot of the 27μm QD laser biased at 15mA can be seen in figure 4.9.

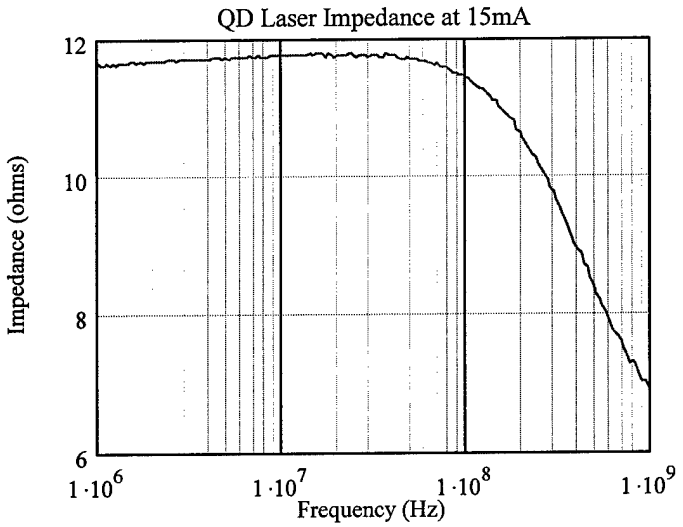

Figure 4.9. Impedance behavior of a 27μm QD laser biased at 15mA—threshold was 48mA.

From figure 4.9, we can see that the QD laser impedance varied from nearly 12Ω down to approximately 7Ω in the frequency range of 1MHz to 1GHz. As we continue to decrease the bias level, the impedance of the laser will become significant when compared to the 860Ω of resistance used in the high frequency bias circuit. When this occurs, we have to

begin using the low frequency bias circuit with the larger resistors. Figure 4.10 illustrates the impedance behavior of the 27μm QD laser biased at 2mA.

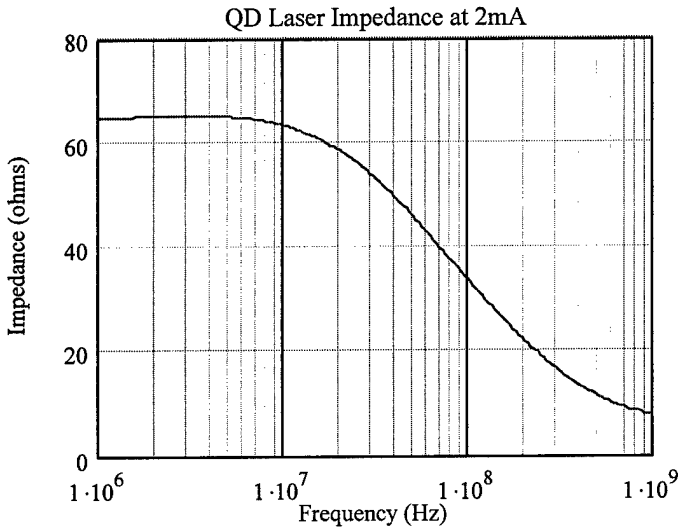

Figure 4.10. Impedance behavior of a 27μm QD laser biased at 2mA—threshold was 48mA.

From this figure, we see that the impedance of the QD laser is around 67Ω at 1MHz and around 7Ω at 1GHz. Thus, we need to use the low frequency bias circuit to yield a constant modulation current at this bias level. The next section will examine how constant our modulation currents are for the low and high frequency bias circuits at the 2mA and 15mA bias levels respectively.

4.4 Phase II: Model

During this phase of the design process, we again developed a MathCad program capable of modeling the small-signal modulation current of the laser diode as a function of frequency. A flow chart for the MathCad program used to model the modulation current and the program itself can be seen in Appendix B. The components used in the low frequency and high frequency bias circuits can be seen in tables 4.1 and 4.2.

Low Frequency Bias Tee Circuit Components

Component	Dimensions	Size	#used
Resistor	0603	3.3kΩ	2
Capacitor	0603	.1μF	1
Inductor	1206	100μH	1
		10μH	3

Table 4.1. The components used in the low frequency bias tee circuit.

High Frequency Bias Tee Circuit Components

Component	Dimensions	Size	#used
Resistor	0805	430Ω	2
Capacitor	0603	.1μF	1
Inductor	1206	100μH	1
		10μH	3

Table 4.2. The components used in the high frequency bias tee circuit.

As previously mentioned, the only difference between the low frequency bias tee circuit and the high frequency bias tee circuits are the resistors used. To measure the performance of the low frequency and high frequency bias circuits, we plotted the small-signal modulation current of each of these bias circuits at the above threshold value of 70mA for the 27μm QD laser; the plots can be seen in figures 4.11 and 4.12. We also included the modeled modulation currents for the QD laser biased at 2mA and 15mA on the low frequency bias circuit plot and the high frequency bias circuit plot respectively. This is done

in order to illustrate how constant the modulation currents remain at biases well below the calibration curve bias of 70mA—ideally, we would like them to be the same.

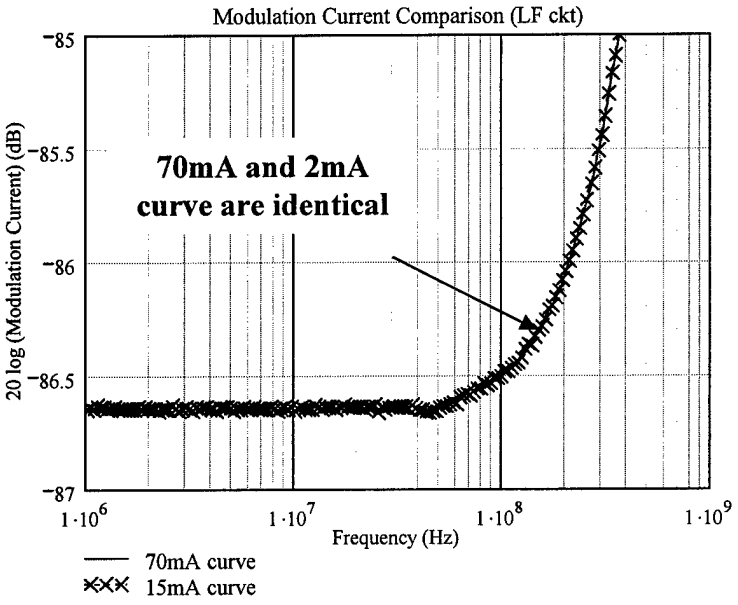

Figure 4.11. Modulation current comparison for the 70mA and 2mA bias levels of the 27μm QD laser.

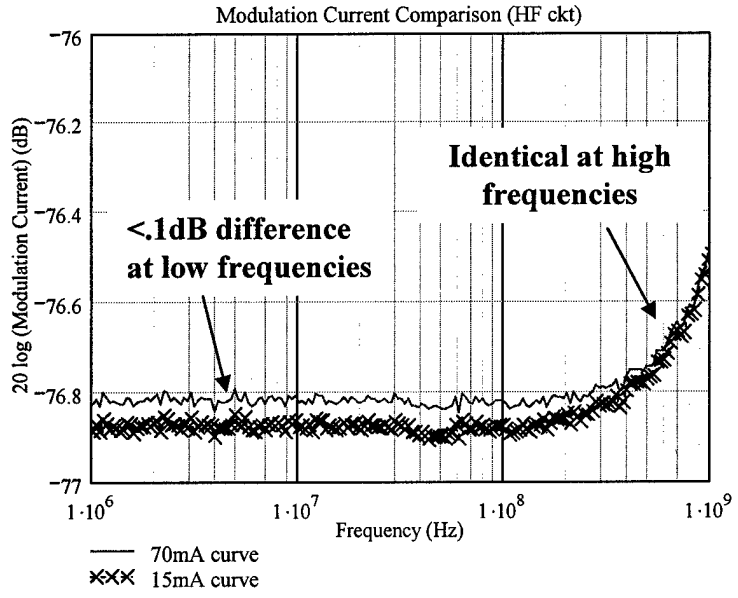

Figure 4.12. Modulation current comparison for the 70mA and 15mA bias levels of the 27μm QD laser.

The modulation currents in each of these plots are displayed in dB to illustrate the expected amount of change we would expect to see in the optical response curves due to a

change in the modulation current—the responsivity[1] of our photo-diode is .9 at the 1.3μm wavelength, which makes the photo current produced by the photo-diode very similar (if the responsivity were 1 they would be identical) in magnitude to the modulation current delivered to the laser. From figure 4.11, we see that the modeled modulation current of the 70mA calibration curve is identical to the modeled modulation current with the laser biased at 2mA. However, in figure 4.12, we see that the modeled modulation current of the 70mA calibration curve is actually greater than the modeled modulation current at the below threshold laser bias of 15mA—due to the increasing laser impedance at a lower bias. The disparities are not significant at the 15mA bias, but reducing the laser bias below 15mA is expected to yield errors in the lifetime data.

4.5 Phase III: Design

During this design phase, we used the same microwave board layout as in the first design. The microwave board layout can be seen in figure 4.13, and the component placement for both the high frequency and low frequency bias tee circuits can be seen in figure 4.14.

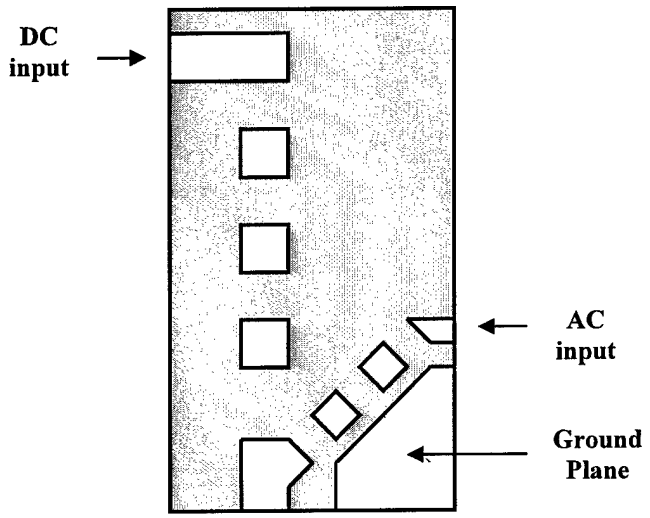

Figure 4.13. Microwave board layout for the low and high frequency bias tee circuits.

[1] The responsivity of a photo-diode is equal to the photo-current produced by the photo-diode divided by the power incident on the photo-diode: $R = I_{ph}/P_{inc}$ (A/W) [2].

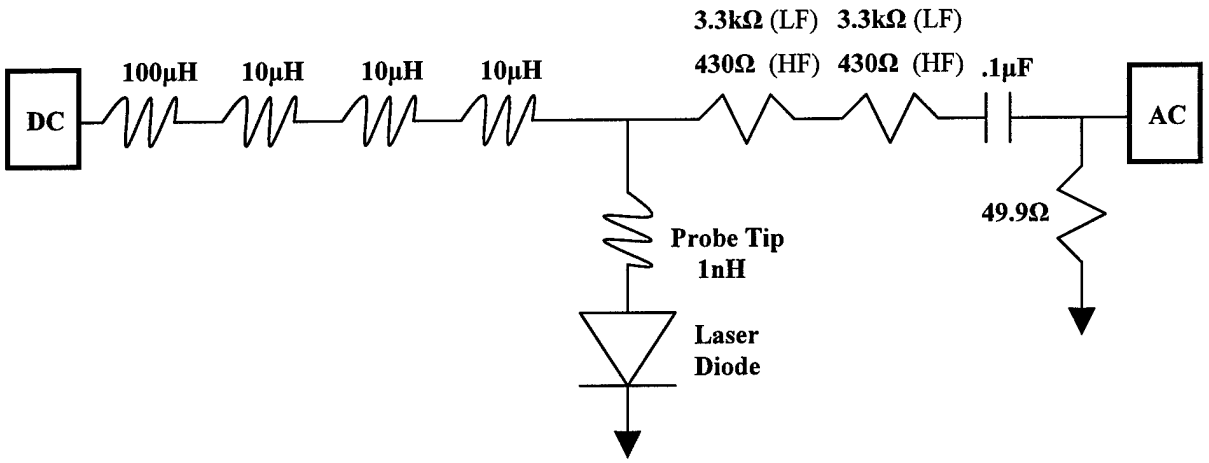

Figure 4.14. Low frequency (LF) and high frequency (HF) bias tee circuit component placement.

Since the microwave board layout was the same as the one used in the data sheet design, we just exchanged the components and began testing the low frequency and high frequency bias tee circuits.

4.6 Phase IV: Testing and Results

The first test we submitted the bias tee circuits to was the calibration curve. The calibration curve for the low frequency bias circuit is found in figure 4.15 and the calibration curve for the high frequency bias circuit is found in figure 4.16.

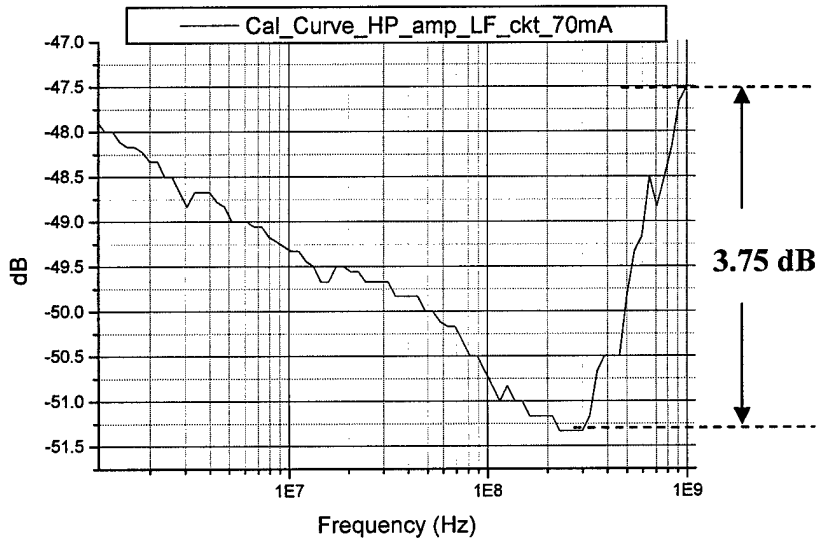

Figure 4.15. Low frequency circuit calibration curve taken at 70mA with 25dB HP amplifier.

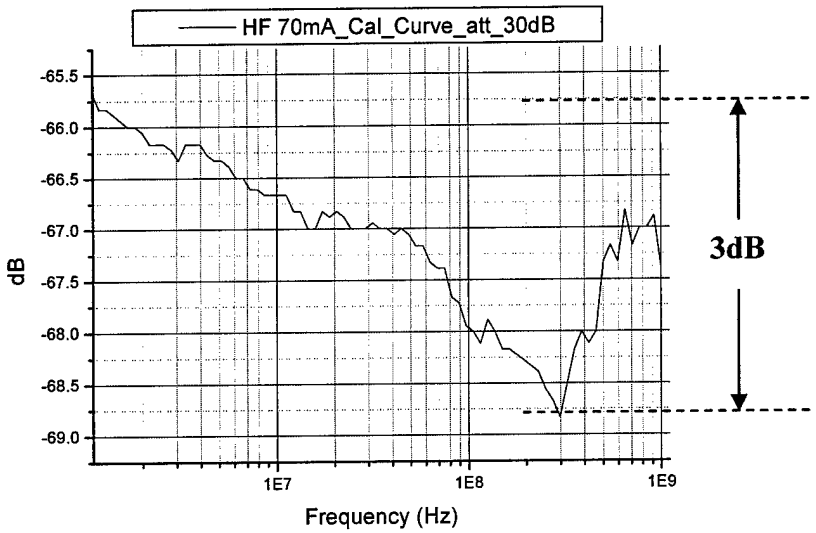

Figure 4.16. High frequency circuit calibration curve taken at 70mA with 25dB HP amplifier.

The calibration curves found in figures 4.15 and 4.16 look very good compared to the calibration curve seen in chapter 3, which had 12dB of change (figure 3.8 pg 51). The calibration curve for the low frequency bias circuit yields only 3.75dB of change from 1MHz to 1GHz, and the high frequency bias circuit yields only 3dB of change from 1MHz to 1GHz; most of the change in these calibration curves is coming from the amplifier response (illustrated in figure 4.18). However, there are differences in the calibration curve and the Hewlett Packard (HP) amplifier response curves, such as the gradual decline in the calibration curve from 1MHz to 200MHz (which is not seen in the amplifier response curve), and the ~1.5dB dip in the amplifier response curve from 600MHz to 1GHz (which is not identically followed by the calibration curves). There are a variety of other sources in the experimental setup which could be contributing to the disparities between the calibration curves and the amplifier response curve (cable losses, power fluctuations from the network analyzer, and the photo-detector circuit), so we went ahead with the next test—taking below threshold optical response curves.

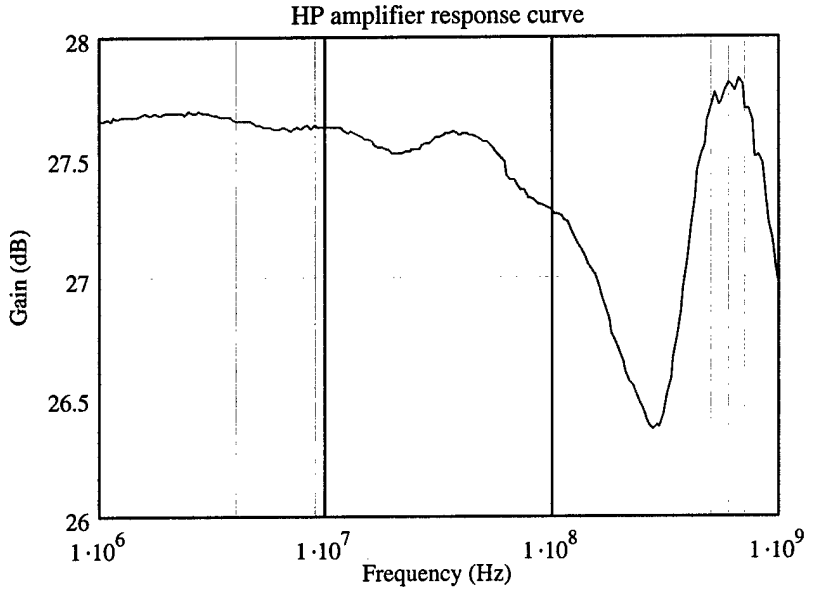

Figure 4.17. 25dB HP amplifier response.

We took a below threshold optical response curve using both the low frequency and the high frequency bias circuits on a 27μm quantum dot (QD) laser biased at 26mA. We then subtracted the calibration curve taken with the low frequency circuit (figure 4.16) and the calibration curve taken with the high frequency circuit (figure 4.17) from their below threshold optical response curves to yield the single-pole response curves seen in figures 4.18 and 4.19. Both curves maintained a reasonably flat region from 1MHz to 100MHz and a roll-off which is slightly steeper than the expected 20dB per decade roll-off from the single-pole response—the solid line is the single-pole fit. The steeper than 20dB per decade roll-off is not understood at this time; it could be coming from the amplifier, or just the laser dynamics itself. However, the resulting below threshold optical response curves and the modeled modulation currents do give us confidence in these bias circuits, and with the help of a new low noise Mitech amplifier possessing a 1MHz to 1GHz bandwidth, we feel the below threshold optical curves will improve even further.

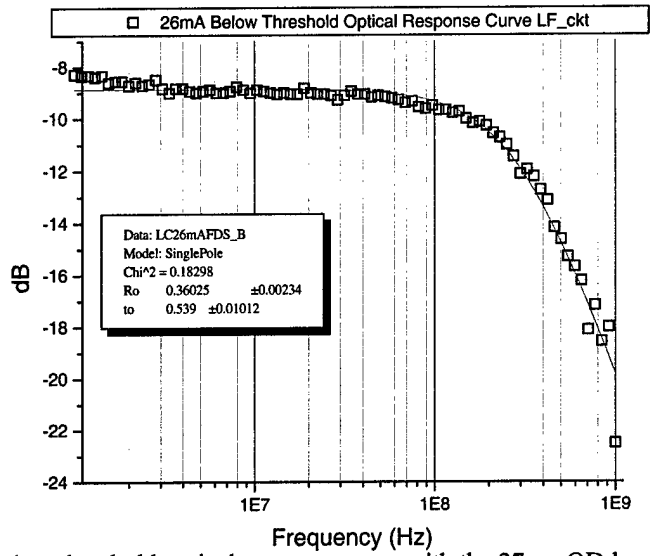

Figure 4.18. Below threshold optical response curve with the 27μm QD laser biased at 26mA using the low frequency bias circuit and the HP amplifier.

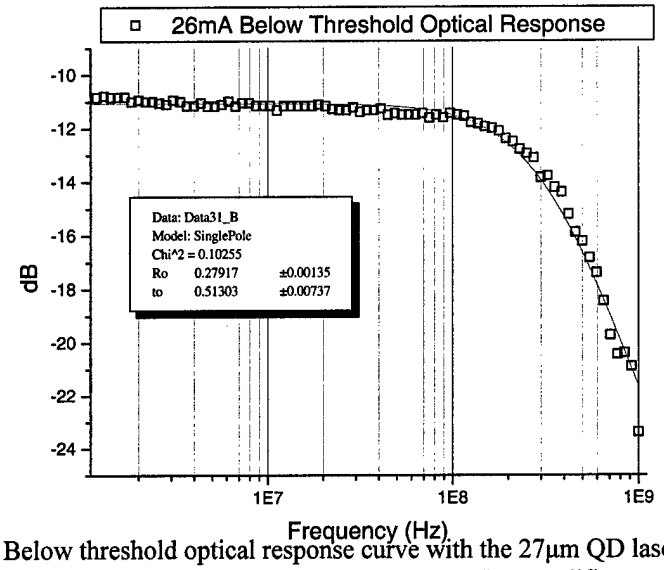

Figure 4.19. Below threshold optical response curve with the 27μm QD laser biased at 26mA using the high frequency bias circuit and the HP amplifier.

4.7 Improvements

As previously mentioned, we would like to use a new low noise Mitech amplifier with at 1MHz to 1GHz bandwidth to perform measurements in the future. The necessity of this amplifier is revealed when we examine calibration curves taken with the HP amplifier (figure 4.20) and calibration curves taken with our low noise Mitech amplifier with 10MHz

to 1GHz bandwidth (figure 4.21). We took calibration curves using each of these amplifiers using the 27μm QD laser biased at 66mA and again at 70mA. Ideally, we would like to see exact replicas of the calibration curves running parallel to each other (70mA curve above the 66mA curve) across the entire frequency range; the 70mA curve should be on top due to the increased optical power at the 70mA operating point, and the curves should be parallel to each other as long as the amplifier characteristics do not change with different input powers. This type of behavior is not seen with the 25dB HP amplifier (it is sensitive to different input powers); however, we do see nearly ideal behavior from a 40dB low noise Mitech amplifier. On a final note, we believe the increased predictability of the low noise Mitech amplifier will yield more accurate below threshold optical response curves.

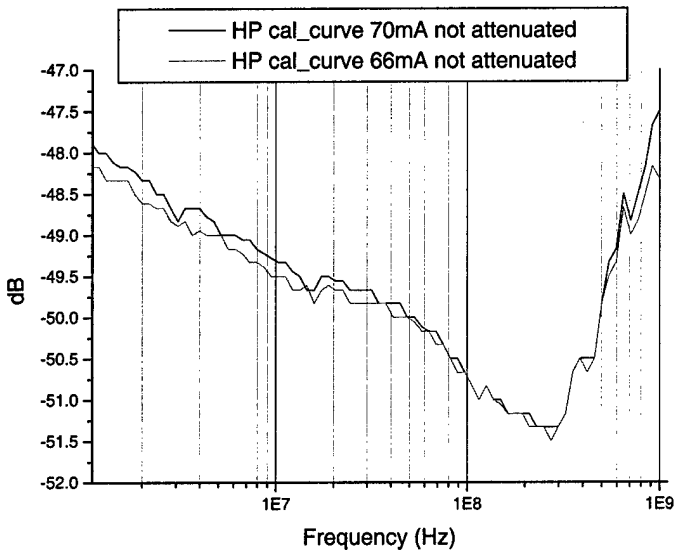

Figure 4.21. Calibration curves taken on the 27μm QD laser biased at 66mA and 70mA using the low frequency bias circuit and the 25dB HP amplifier.

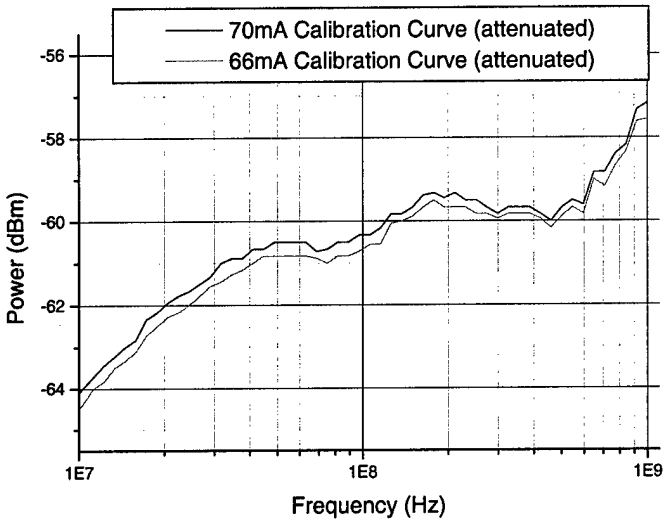

Figure 4.21. Calibration curves taken on the 27μm QD laser biased at 66mA and 70mA using the low frequency bias circuit and the 40dB low noise Mitech amplifier.

References--Chapter 4

[1] M.M Radmanesh, "Radio Frequency and Microwave Electronics," Prentice Hall, 2001.

[2] P. Bhattacharya, "Semiconductor Optoelectronic Devices," Prentice Hall, 1997.

[3] J.M. Pikal, "Temperature Dependence of Carrier Lifetime, Recombination, and Gain in 1.3μm InAsP/InGaAsP Multiple Quantum Well Lasers," Dissertation, Aug. 1999.

Chapter 5

Conclusion

The objective of our work was to design a bias circuit capable of delivering a constant, small-signal modulation current to a semiconductor laser from 1MHz to 1GHz; thereby, allowing us to measure the small-signal optical response of the laser in this regime. We first approached this design through modeling the components of the bias tee circuit using information on the components' parasitics retrieved from data sheets, and using our best guess at the parasitics that were not available. Once we modeled the impedance behavior of our bias tee circuit, we then tested the bias tee circuit on a theoretical model of a semiconductor laser to see how constant the modulation current was. According to our model, we did obtain a constant modulation current delivery to the semiconductor laser; however, this was because our assumption on the parasitic capacitance of our resistors was an order of magnitude low. Unaware of this fact, we moved to design and test the bias tee circuit.

After submitting the bias tee circuit to its first test—the calibration curve—we felt there was something wrong with our model; the first calibration curve yielded 12dB of rise from 200MHz to 1GHz. We did find that the HP amplifier we were using did have some undesireable, nonlinear characteristics; however, with only a total of 1.5dB of change in the amplifier response from 1MHz to 1GHz, we knew it was not solely responsible for the 12dB rise in our calibration curve. We suspected an increasing modulation current was being delivered to our laser. For this reason, we pursued another design approach of the bias tee circuit.

In the second design approach, we used experimentally measured impedances for the QD laser and the components used in the bias tee circuit—we moved from a theoretical

impedance model to an experimentally measured impedance model. From the resistor impedance measurements, we discovered why our calibration curve in the first design yielded 12dB of rise from 200MHz to 1GHz. The parasitic capacitance of our resistors limited the bandwidth of the 5.1kΩ resistors used in the first bias tee circuit design to ~200MHz, which caused the modulation current delivered to the semiconductor laser to continually increase above 200MHz. It was at this point that we decided to design two bias tee circuits: one used at low bias levels where the impedance of the laser is large and the single-pole, small-signal optical response resides at lower frequencies (~1MHz to ~100MHz); and one used at higher bias levels where the impedance of the laser is low and the single-pole, small-signal optical response resides at higher frequencies (~100MHz to ~1GHz). Through breaking the design into two different bias circuits, we were able to take advantage of the laser's low impedance at high biases to get around the low bandwidth problem associated with our resistors.

With the new impedance model, we selected components for both bias circuits, which were capable of delivering a constant modulation current to a semiconductor laser over the frequency regimes they are intended to capture the single-pole, small-signal optical response of the laser. With good results coming from our model, we moved to design and test the two bias circuits. The results of the first test—calibration curves—showed great improvement: the low frequency bias circuit only yielded 3.75dB of change and the high frequency bias circuit only yielded 3dB of change. With good calibration curve results, we moved to the final test—below threshold optical response curves.

Both bias circuits were tested on a 27μm wide QD laser biased at 26mA (threshold current was 48mA), and each reflected a reasonably, nice single-pole response. There were some fluctuations present both in the flat region and in the single-pole response; however, we

feel that a new low noise Mitech amplifier with a 1MHz to 1GHz bandwidth can help reduce these fluctuations. Overall, the results of both tests (calibration curve and below threshold optical response curve) and our modeled results give us confidence that a constant modulation current was delivered to the laser by both bias tee circuits.

Appendix A

Flow Chart and MathCad Program for Data Sheet Design of the Bias Tee Circuit

Define the frequency range of operation (1MHz to 1GHz) and ensure we maintain the same number of points in each decade.

↓

Define the impedance of the laser diode.
$\mathbf{R_{sd}}$ = series resistance of cladding layers ~ 4Ω
$\mathbf{R_d}$ = differential resistance of the p-n junction
$\mathbf{C_d}$ = differential capacitance of the active region

↓

Define the impedance of the probe tip—neglect the resistance.
$\mathbf{L_{pt}}$ = inductance of 2mm probe tip ~ 1nH

↓

Define the impedance of the inductors used.
Input the following values:
SRF = self resonant frequency
$\mathbf{R_p(f)}$ = parasitic resistance value
L = nominal inductance value
Determine the parasitic capacitance $\mathbf{C_p}$ value from SRF and L.
High frequency model impedance is:

$$Z_{LHF} = \left[\frac{1}{R_p(f) + j\omega L} + j\omega C_p \right]^{-1}$$

↓

Define the impedance of the capacitors used.
Input the following values:
$\mathbf{R_{cp}}$ = parasitic resistance value
$\mathbf{L_{cp}}$ = parasitic inductance value
C = nominal capacitance value
High frequency model impedance is:

$$Z_{CHF} = \left[\frac{1}{j\omega C} + j\omega L_{cp} + R_{cp} \right]$$

↓

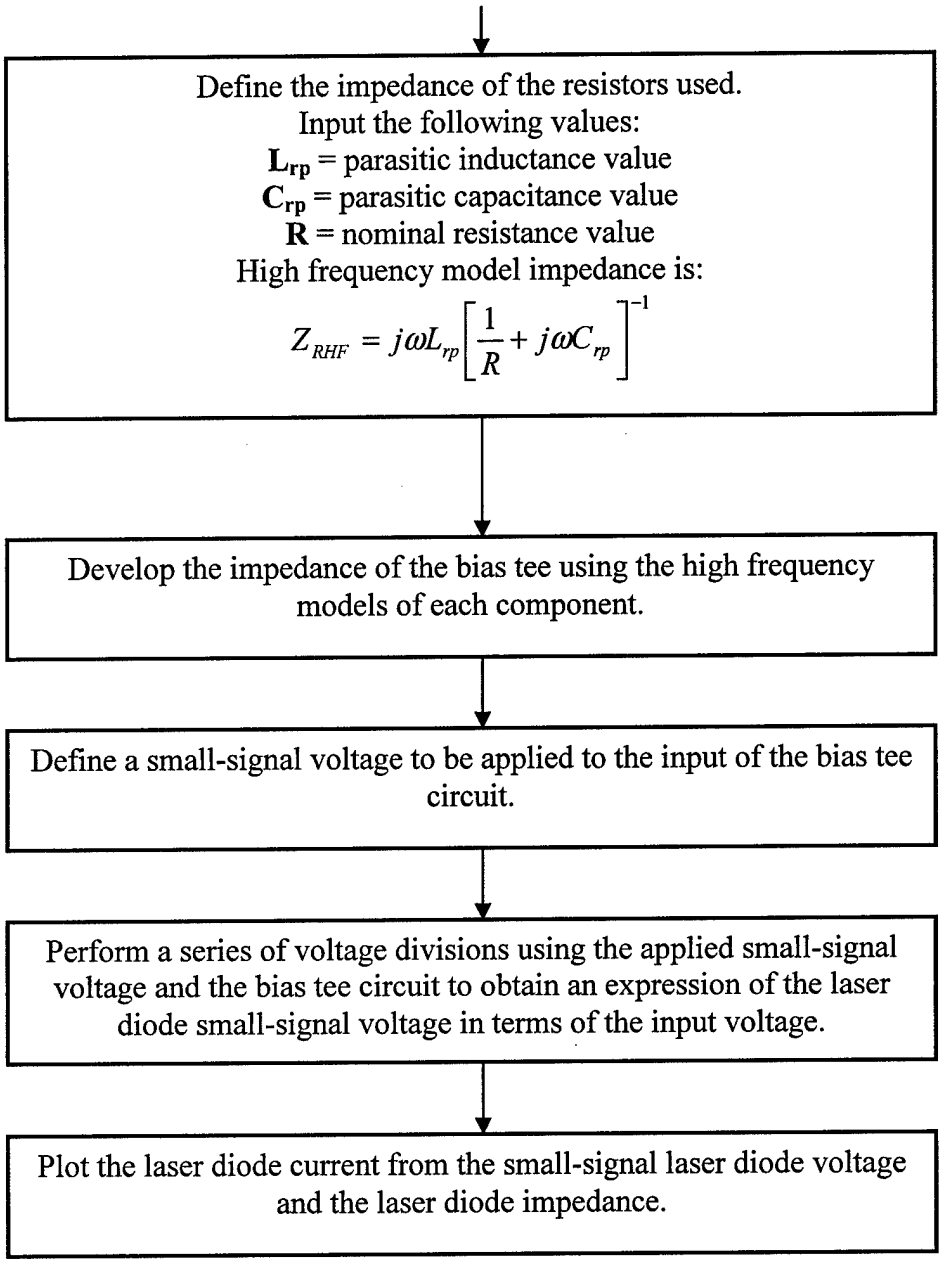

Figure A1. Flow chart for MathCad program used to model the small-signal modulation current delivered to the laser diode.

Frequency and characteristic impedance definitions:

$lf := 0, 0.0025 .. 3.99 \qquad w(lf) := 2 \cdot \pi \cdot 10^{(lf+5)}$

Laser diode definitions:

$Rsd := 4.0 \qquad Rd := 250 \qquad Cd := 5.0 \cdot 10^{-10}$

$ZLD(lf) := Rsd + \left(\frac{1}{Rd} + i \cdot w(lf) \cdot Cd \right)^{-1}$ **Differential carrier lifetime:** $Rd \cdot Cd = 1.25 \times 10^{-7}$

Probe tip impedance definition: **inductance value is for a 2mm probe tip**

$L_{pt} := 1 \cdot 10^{-9} \qquad ZPT(lf) := i \cdot w(lf) \cdot L_{pt}$

Inductor impedance definitions: **need SRF value, parasitic resistance, and inductance value to complete the high frequency model.**

$SRF1 := 2 \cdot \pi \cdot 120 \cdot 10^{6} \qquad Rp1(lf) := .001124 \sqrt{\frac{w(lf)}{2\pi}} \qquad L1 := 6.8 \cdot 10^{-6} \qquad Q1 := 38$

$SRF2 := 2\pi \cdot 105 \cdot 10^{6} \qquad Rp2(lf) := .001653 \sqrt{\frac{w(lf)}{2\pi}} \qquad L2 := 10 \cdot 10^{-6} \qquad Q2 := 38$

Determine the parasitic capacitance values from the SRF's:

$Cp1 := \left(SRF1^2 \cdot L1\right)^{-1} \qquad Cp2 := \left(SRF2^2 \cdot L2\right)^{-1}$

$Cp1 = 2.587 \times 10^{-13} \qquad Cp2 = 2.298 \times 10^{-13}$

Check to see if the SRF's and Q's match values stated above for each inductor:

SRF1: $\frac{1}{2 \cdot \pi \cdot \sqrt{L1 \cdot Cp1}} = 1.2 \times 10^{8}$ **Q1:** $\frac{L1 \cdot 2\pi 10^{6}}{Rp1(1)} = 38.012$

SRF2: $\frac{1}{2 \cdot \pi \cdot \sqrt{L2 \cdot Cp2}} = 1.05 \times 10^{8}$ **Q2:** $\frac{L2 \cdot 2\pi 10^{6}}{Rp2(1)} = 38.011$

Define the impedance of each inductor using their high frequency models:

$$ZL1(lf) := \left(\frac{1}{Rp1(lf) + i \cdot w(lf) \cdot L1} + i \cdot w(lf) \cdot Cp1 \right)^{-1} \qquad ZL2(lf) := \left(\frac{1}{Rp2(lf) + i \cdot w(lf) \cdot L2} + i \cdot w(lf) \cdot Cp2 \right)^{-1}$$

Define the total impedance of the inductive network:

$$ZL(w) := 1\,ZL1(w) + 3\,ZL2(w)$$

<u>Capacitor impedance definitions:</u> need paracitic resistance, parasitic lead inductance, and capacitance values to complete the high frequency model.

$$R_{cp} := .07 \qquad L_{cp} := 1.6 \cdot 10^{-9} \qquad C1 := .1 \cdot 10^{-6}$$

Check the resonant frequency with the data sheet figure:

$$\frac{1}{2 \cdot \pi \cdot \sqrt{C1 \cdot L_{cp}}} = 1.258 \times 10^{7}$$

Define the impedance of the capacitor using its high frequency model:

$$ZC1(lf) := \frac{1}{i \cdot w(lf) \cdot C1} + i \cdot w(lf) \cdot L_{cp} + R_{cp}$$

Define the total impedance of the capacitive network:

$$ZC(w) := ZC1(w)$$

<u>Capacitor impedance definitions:</u> need paracitic lead inductance, parasitic capacitance, and the resitance values to complete the high frequency model.

$$L_{rp} := 1.0 \cdot 10^{-10} \qquad C_{rp} := 0.01 \cdot 10^{-12} \qquad R := 5100$$

Define the impedance of the resistor using its high frequency model:

$$ZR1(lf) := \left(\frac{1}{R + i \cdot w(lf) \cdot L_{rp}} + i \cdot w(lf) \cdot C_{rp} \right)^{-1}$$

Define the total impedance of the resistive network:

$$ZR(w) := 2\,ZR1(w)$$

Now, we have a series of impedance networks defined ZLD, ZPT, ZL, ZC, and ZR for the laser diode, probe tip, inductive network, capacitive network, and resistive network respectively.

The next step is to move toward obtaining a modulation voltage across the laser diode from a modulation voltage placed at the input of the bias tee--at the 50 Ω shunt resistor. We will do this through a series of voltage divider expressions until we arrive at an expression of the laser diode voltage as a function of the input voltage. Once we do this, we can plot the modulation current delivered to the laser diode.

Z1 is the impedance of the inductors in parallel with the probe tip and laser.

$$Z1(lf) := \left(\frac{1}{ZL(lf)} + \frac{1}{ZLD(lf) + ZPT(lf)} \right)^{-1}$$

ZBT is the total impedance of the bias tee circuit, including the probe tip inductance and the laser diode impedance .

$$ZBT(lf) := ZR(lf) + ZC(lf) + Z1(lf)$$

Zin is the impedance of the 50 Ω shunt resistor in parallel with the impedance of the bias tee circuit, including the probe tip impedance and the laser diode impedance--the total input impedance seen by the network analyzer.

$$Zin(lf) := \left(\frac{1}{50} + \frac{1}{ZBT(lf)} \right)^{-1}$$

Now, define the small signal voltage and determine the power of the signal applied

$Vin := 0.44721359$ $\qquad P_{in} := 10 \cdot \log\left[\frac{\left(\frac{Vin}{2} \right)^2}{50} \Big/ 0.001 \right]$ $\qquad P_{in} = -1.068 \times 10^{-7}$ **dBm**

Now, define the voltage seen at the probe tip and call it V1--a voltage divider expression using Z1, ZC, and ZC.

$$V1(lf) := Vin \cdot \frac{Z1(lf)}{ZC(lf) + ZR(lf) + Z1(lf)}$$

Use a voltage divider expression again involving the voltage at the probe tip (V1) and the impedances of the laser diode and probe tip.

$$Vd(lf) := V1(lf) \cdot \frac{ZLD(lf)}{ZPT(lf) + ZLD(lf)}$$

Now, define the magnitude of the laser diode current.

$$Id(lf) := \left| \frac{Vd(lf)}{ZLD(lf)} \right|$$

Plot the magnitude of the small-signal modulation current delivered to the laser diode.

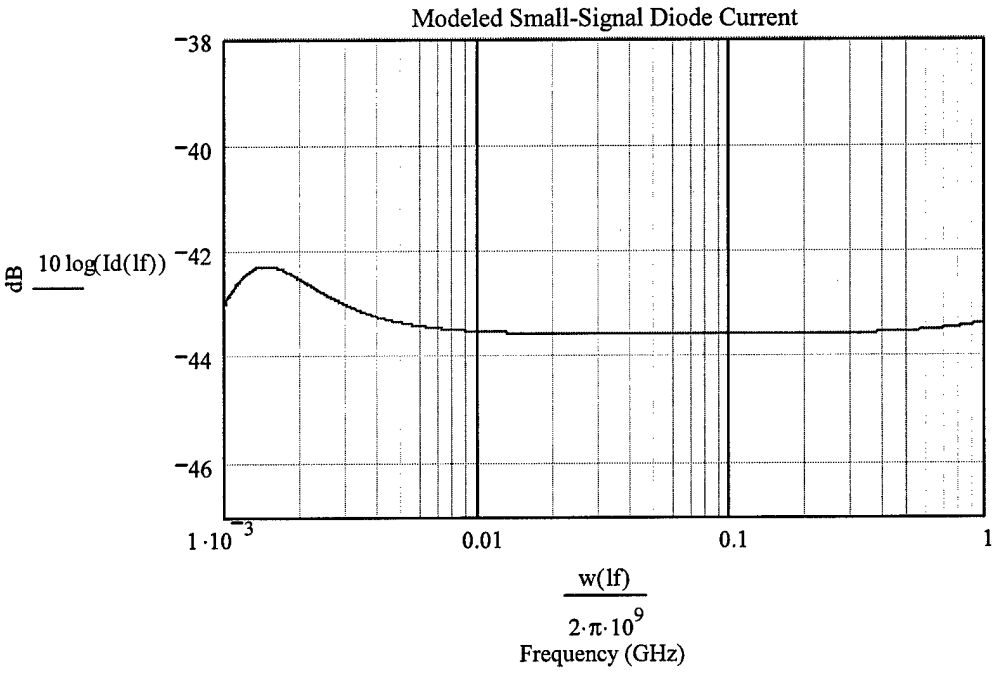

Appendix B

Flow Chart and MathCad Program for Experimentally Measured Impedance Design of the Bias Tee Circuit

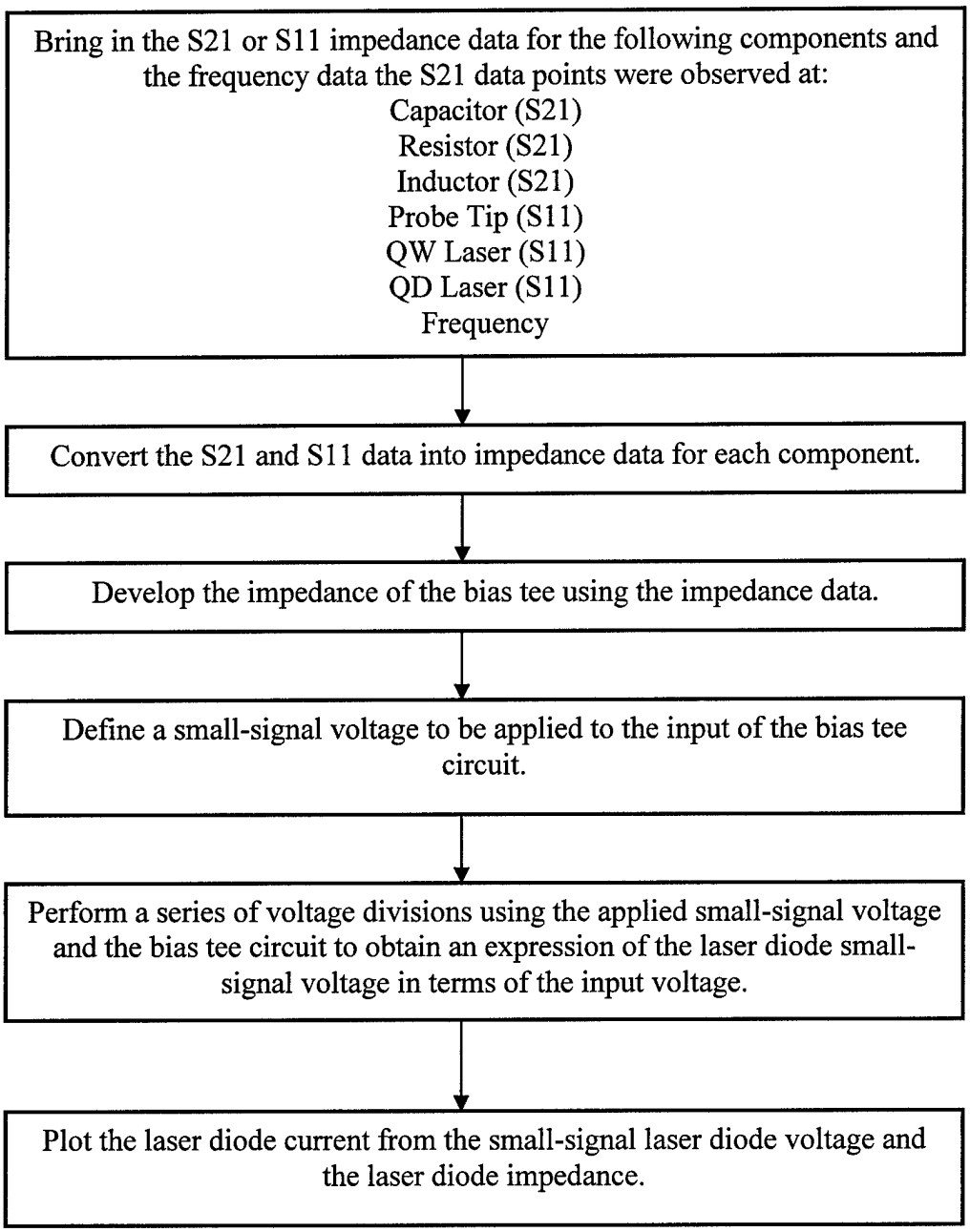

Figure B1. Flow chart for MathCad program used to model the small-signal modulation current delivered to the laser diode.

Capacitor Impedance Data

Cap1_transmag := READPRN("capacitor_mag_and_phase_S11_and_S21_data\10nF_0805_S21_mag_data.txt")

Cap1_transphase := READPRN("capacitor_mag_and_phase_S11_and_S21_data\10nF_0805_S21_phase_data.txt")

Resistor Data

Res1_transmag := READPRN("resistor_mag_and_phase_S11_and_S21_data\430ohm_0805_panasonic_S21_mag_data.txt")

Res1_transphase := READPRN("resistor_mag_and_phase_S11_and_S21_data\430ohm_0805_panasonic_S21_phase_data.txt")

Res2_transmag := READPRN("resistor_mag_and_phase_S11_and_S21_data\3.3kohm_0603_panasonic_S21_mag_data.txt")

Res2_transphase := READPRN("resistor_mag_and_phase_S11_and_S21_data\3.3kohm_0603_panasonic_S21_mag_data.txt")

Inductor Data

Ind1_transmag := READPRN("inductor_mag_and_phase_S11_and_S21_data\100uH_jwmiller_S21_mag_data.txt")

Ind1_transphase := READPRN("inductor_mag_and_phase_S11_and_S21_data\100uH_jwmiller_S21_phase_data.txt")

Ind2_transmag := READPRN("inductor_mag_and_phase_S11_and_S21_data\10uH_jwmiller_S21_mag_data.txt")

Ind2_transphase := READPRN("inductor_mag_and_phase_S11_and_S21_data\10uH_jwmiller_S21_phase_data.txt")

Ind3_transmag := READPRN("inductor_mag_and_phase_S11_and_S21_data\10uH_jwmiller_S21_mag_data.txt")

Ind3_transphase := READPRN("inductor_mag_and_phase_S11_and_S21_data\10uH_jwmiller_S21_phase_data.txt")

Ind4_transmag := READPRN("inductor_mag_and_phase_S11_and_S21_data\1.5uH_jwmiller_S21_mag_data.txt")

Ind4_transphase := READPRN("inductor_mag_and_phase_S11_and_S21_data\1.5uH_jwmiller_S21_phase_data.txt")

Probe Tip Data:

Ptip_refl := READPRN("1p5mm_probe_tip_inductance_data.txt")

QW Laser Data:

QWL_refl := READPRN("QW_Laser_Impedance\2.txt")

QD Laser Data:

QDL1_refl:= READPRN("QD_Laser_Impedance\QD70mA.txt")

QDL2_refl:= READPRN("QD_Laser_Impedance\QD7mA.txt")

Frequency Data:

freq := READPRN("Frequency_Data_1MHz_to_2GHz.txt")

Define the characteristic impedance (50 Ω) and set up the frequency--the frequency must be read from the array, thus requiring i to keep track of the frequency point where the impedance data point was observed:

Zo := 50 f := freq i := 0.. 200

Capacitor S21 to Impedance Conversion:

$$Cap1\_S21_i := 10^{\frac{Cap1\_transmag_i}{20}} \cdot \cos\left(\frac{\pi}{180} Cap1\_transphase_i\right) + i \cdot 10^{\frac{Cap1\_transmag_i}{20}} \cdot \sin\left(\frac{\pi}{180} Cap1\_transphase_i\right)$$

$$Cap1\_Z_i := Zo \cdot \frac{2 \cdot \left(1 - Cap1\_S21_i\right)}{Cap1\_S21_i}$$

Resistor S21 to Impedance Conversion:

$$Res1\_S21_i := 10^{\frac{Res1\_transmag_i}{20}} \cdot \cos\left(\frac{\pi}{180} Res1\_transphase_i\right) + i \cdot 10^{\frac{Res1\_transmag_i}{20}} \cdot \sin\left(\frac{\pi}{180} Res1\_transphase_i\right)$$

$$Res1\_Z_i := Zo \cdot \frac{2 \cdot \left(1 - Res1\_S21_i\right)}{Res1\_S21_i}$$

$$Res2\_S21_i := 10^{\frac{Res2\_transmag_i}{20}} \cdot \cos\left(\frac{\pi}{180} Res2\_transphase_i\right) + i \cdot 10^{\frac{Res2\_transmag_i}{20}} \cdot \sin\left(\frac{\pi}{180} Res2\_transphase_i\right)$$

$$Res2\_Z_i := Zo \cdot \frac{2 \cdot \left(1 - Res2\_S21_i\right)}{Res2\_S21_i}$$

Inductor S21 to Impedance Conversion:

$$Ind1\_S21_i := 10^{\frac{Ind1\_transmag_i}{20}} \cdot \cos\left(\frac{\pi}{180} Ind1\_transphase_i\right) + i \cdot 10^{\frac{Ind1\_transmag_i}{20}} \cdot \sin\left(\frac{\pi}{180} Ind1\_transphase_i\right)$$

$$Ind1\_Z_i := Zo \cdot \frac{2 \cdot \left(1 - Ind1\_S21_i\right)}{Ind1\_S21_i}$$

$$Ind2\_S21_i := 10^{\frac{Ind2\_transmag_i}{20}} \cdot \cos\left(\frac{\pi}{180} Ind2\_transphase_i\right) + i \cdot 10^{\frac{Ind2\_transmag_i}{20}} \cdot \sin\left(\frac{\pi}{180} Ind2\_transphase_i\right)$$

$$Ind2\_Z_i := Zo \cdot \frac{2 \cdot (1 - Ind2\_S21_i)}{Ind2\_S21_i}$$

$$Ind3\_S21_i := 10^{\frac{Ind3\_transmag_i}{20}} \cdot \cos\left(\frac{\pi}{180} Ind3\_transphase_i\right) + i \cdot 10^{\frac{Ind3\_transmag_i}{20}} \cdot \sin\left(\frac{\pi}{180} Ind3\_transphase_i\right)$$

$$Ind3\_Z_i := Zo \cdot \frac{2 \cdot (1 - Ind3\_S21_i)}{Ind3\_S21_i}$$

$$Ind4\_S21_i := 10^{\frac{Ind4\_transmag_i}{20}} \cdot \cos\left(\frac{\pi}{180} Ind4\_transphase_i\right) + i \cdot 10^{\frac{Ind4\_transmag_i}{20}} \cdot \sin\left(\frac{\pi}{180} Ind4\_transphase_i\right)$$

$$Ind4\_Z_i := Zo \cdot \frac{2 \cdot (1 - Ind4\_S21_i)}{Ind4\_S21_i}$$

Probe Tip S11 to Impedance Conversion:

$$Ptip\_S11_i := Ptip\_refl_{i,0} + i \cdot Ptip\_refl_{i,1} \qquad Ptip\_Z_i := Zo \cdot \frac{1 + Ptip\_S11_i}{1 - Ptip\_S11_i}$$

QW Laser S11 to Impedance Conversion:

$$QWL\_S11_i := QWL\_refl_{i,0} + i \cdot QWL\_refl_{i,1} \qquad QWL\_Z_i := Zo \cdot \frac{1 + QWL\_S11_i}{1 - QWL\_S11_i}$$

QD Laser S11 to Impedance Conversion:

$$QDL1\_S11_i := QDL1\_refl_{i,0} + i \cdot QDL1\_refl_{i,1} \qquad QDL1\_Z_i := Zo \cdot \frac{1 + QDL1\_S11_i}{1 - QDL1\_S11_i}$$

$$QDL2\_S11_i := QDL2\_refl_{i,0} + i \cdot QDL1\_refl_{i,1} \qquad QDL2\_Z_i := Zo \cdot \frac{1 + QDL2\_S11_i}{1 - QDL2\_S11_i}$$

Now model the modulation current delivered to the laser through placing a small-signal voltage at the input of the bias circuit. From here, we use a series of voltage dividers to obtain the actual small-signal voltage across the laser. Finally, dividing the small signal voltage by the laser impedance, we can examine the small-signal current delivered to the laser.

This is the amplitude of the small-signal voltage applied to the bias circuit; application is just before the 50 ohm resistor.

$Vin := 0.125$

Now, compute the applied power in dBm which will be delivered to the box assuming the impedance remains nearly 50 ohms.

$$P_{dBm} := 10 \cdot \log\left[\frac{\left(\frac{Vin}{\sqrt{2}}\right)^2}{\frac{50}{0.001}}\right] \qquad P_{dBm} = -8.062$$

Now use voltage division to come up with the voltage across the laser diode.

$Zacnetwork_i := 1\,Cap1\_Z_i + 2\,Res1\_Z_i + 0\,Res2\_Z_i$

$Zdcnetwork_i := 2\,Ind1\_Z_i + Ind2\_Z_i + 2\,Ind3\_Z_i + 1\,Ind4\_Z_i$

$ZPtip_i := Ptip\_Z_i$

$$V_{Ptip1_i} := Vin\left[\frac{\frac{(QDL1\_Z_i + ZPtip_i)\cdot Zdcnetwork_i}{QDL1\_Z_i + ZPtip_i + Zdcnetwork_i}}{\frac{(QDL1\_Z_i + ZPtip_i)\cdot Zdcnetwork_i}{QDL1\_Z_i + ZPtip_i + Zdcnetwork_i} + Zacnetwork_i}\right] \qquad V_{laser1_i} := V_{Ptip1_i}\cdot\frac{QDL1\_Z_i}{QDL1\_Z_i + ZPtip_i}$$

$$V_{Ptip2_i} := Vin\left[\frac{\frac{(QDL2\_Z_i + ZPtip_i)\cdot Zdcnetwork_i}{QDL2\_Z_i + ZPtip_i + Zdcnetwork_i}}{\frac{(QDL2\_Z_i + ZPtip_i)\cdot Zdcnetwork_i}{QDL2\_Z_i + ZPtip_i + Zdcnetwork_i} + Zacnetwork_i}\right] \qquad V_{laser2_i} := V_{Ptip2_i}\cdot\frac{QDL2\_Z_i}{QDL2\_Z_i + ZPtip_i}$$

Now that we have the voltage across the laser, determine the current delivered to the laser.

$$I_{laser1_i} := \left|\frac{V_{laser1_i}}{QDL1\_Z_i}\right| \qquad I_{laser2_i} := \left|\frac{V_{laser2_i}}{QDL2\_Z_i}\right|$$

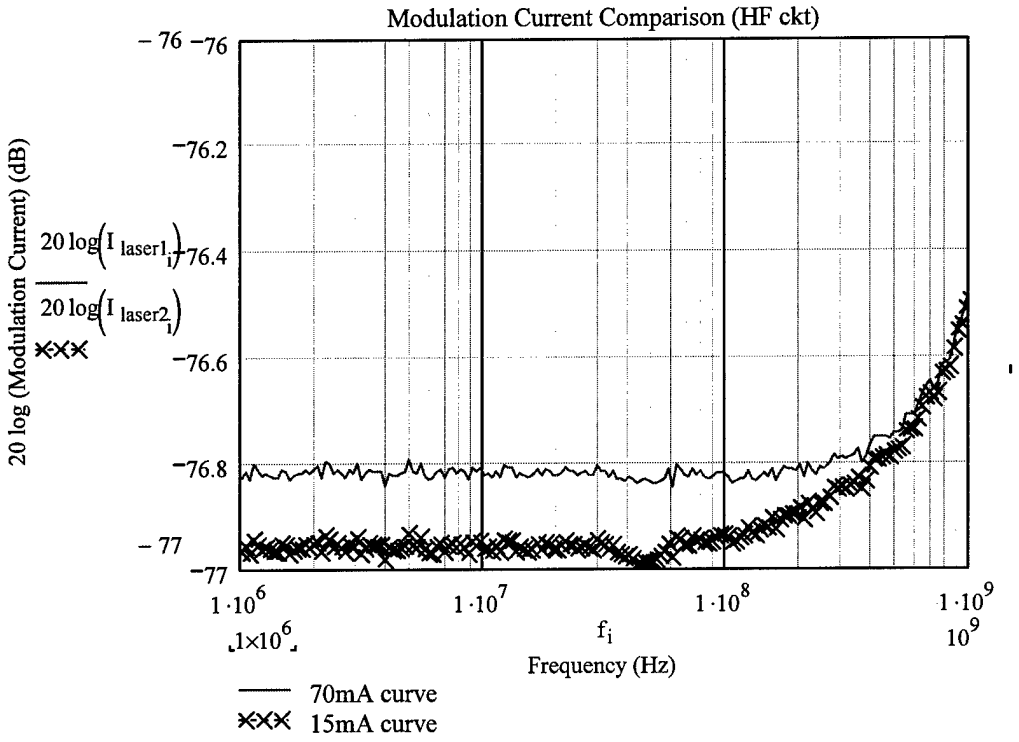
Modulation Current Comparison (HF ckt)
20 log (Modulation Current) (dB)
20 log(I laser1_i)
20 log(I laser2_i)
−76
−76.2
−76.4
−76.6
−76.8
−77
1·10^6
1·10^7
1·10^8
1·10^9
10^9
f_i
Frequency (Hz)
70mA curve
15mA curve